Nasal microbionts differentially colonize and elicit cytokines in human nasal epithelial organoids

Andrea I. Boyd[1,5], Leah A. Kafer[1,5], Isabel F. Escapa[1], Amal Kambal[1], Hira Tariq[1], Susan G. Hilsenbeck[2], Hoa Nguyen-Phuc[1], Anubama Rajan[1,6], Joshua M. Lensmire[1,7], Kathryn A. Patras[1,3], Pedro A. Piedra[1,4], Sarah E. Blutt[1,3], and Katherine P. Lemon*[1,3,4]

[1]Department of Molecular Virology and Microbiology, Baylor College of Medicine, Houston, Texas, USA.

[2]Duncan Cancer Center, Baylor College of Medicine, Houston, Texas, USA.

[3]Alkek Center for Metagenomics and Microbiome Research, Baylor College of Medicine, Houston, Texas, USA.

[4]Division of Infectious Diseases, Texas Children's Hospital and Department of Pediatrics Baylor College of Medicine, Houston, Texas, USA.

[5]These authors contributed equally.

[6]Present address: Department of Medical Sciences and Technology, Indian Institute of Technology, Madras, Chennai, Tamil Nadu, India.

[7]Present address: Immunartes, Chicago, Illinois.

Correspondence: Katherine.lemon@bcm.edu

KEYWORDS: human nasal organoids, HNO, nasal colonization, epithelial innate immune response, bacterial colonization, *Dolosigranulum pigrum*, *Staphylococcus aureus*, MRSA, *Streptococcus pneumoniae*

SUMMARY

Nasal colonization by *Staphylococcus aureus* or *Streptococcus pneumoniae* is associated with an increased risk of infection by these pathobionts, whereas nasal colonization by *Dolosigranulum* species is associated with health. Human nasal epithelial organoids (HNOs) physiologically recapitulate human nasal respiratory epithelium with a robust mucociliary blanket. We reproducibly monocolonized HNOs with these three bacteria for up to 48 hours with varying kinetics across species. HNOs tolerated bacterial monocolonization with localization of bacteria to the mucus layer and minimal cytotoxicity compared to uncolonized HNOs. Human nasal epithelium exhibited both species-specific and general cytokine responses, without induction of type I interferons, consistent with colonization rather than infection. Only live *S. aureus* colonization induced IL-1 family cytokines, suggestive of inflammasome signaling. *D. pigrum* and live *S. aureus* decreased CXCL10, whereas *S. pneumoniae* increased CXCL11, chemokines involved in antimicrobial responses. HNOs are a compelling model system to reveal host-microbe dynamics at the human nasal mucosa.

BRIEF REPORT

There is an urgent need for human-based models that accurately exemplify bacterial nasal colonization. Methicillin-resistant *Staphylococcus aureus* (MRSA) is a leading cause of death due to antimicrobial resistant bacteria globally.[1] The human nasal passages are a primary habitat for *S. aureus* with a third of humans nasally colonized.[2,3] Moreover, *S. aureus* nasal colonization is a risk factor for *S. aureus* infection with ~80% of infection isolates matching the person's nasal isolate.[4-6] In the absence of an effective vaccine[7,8], antibiotic-based *S. aureus* nasal decolonization is the only current strategy to

reduce infections.[9-11] Further, evolutionary analysis shows humans are the major hub for *S. aureus* host switching among mammalian species.[12] Thus, development of human-based models to investigate *S. aureus* nasal colonization is vitally important for the World Health Organizations' One Health, which is "an integrated, unifying approach that aims to sustainably balance and optimize the health of people, animals, and ecosystems."[13] Similarly, *S. pneumoniae* human nasal colonization is the primary reservoir for both invasive pneumococcal disease (IPD) and for pneumococcal transmission.[14] Vaccination has reduced IPD; however, in the absence of a universal vaccine for *S. pneumoniae*, IPD remains a global threat to human health.[1,15] To date, experimental human pneumococcal colonization studies are limited to only a few serotypes[16], and it is unknown whether findings are applicable to a broader range of serotypes, including highly virulent serotypes. In contrast to the threat posed by these two nasal pathobionts, the genus *Dolosigranulum* is frequently associated with healthy cohorts in studies of human nasal microbiota[17] and is inversely associated with *S. aureus* nasal colonization in adults[18-20] and with *S. pneumoniae* nasal colonization in children.[21,22] Furthermore*, D. pigrum* inhibits *S. aureus in vitro*[19] and protects *Galleria mellonella* from *S. aureus* infection *in vivo*[23], supporting its likely role as a nasal mutualist. Using these three species, we demonstrate here that human nasal epithelial organoids (HNOs; aka human nose organoids) are a physiologically relevant model system for elucidating conserved and species-specific human microbiont-epithelial interactions.

HNOs offer more physiological accuracy, genetic diversity, and long-term experimental use than other colonization models. Based on the Sachs *et al*. method for generating Human Airway Organoids[24], HNOs are derived from tissue-resident stem cells collected

using nasal mucosal swabs/washings and propagated *ex vivo* as three-dimensional (3D) organoids that can be frozen and passaged for long-term experimental use. Dispersed 3D organoids plated in monolayers on transwells and differentiated at an air-liquid interface (ALI) accurately recapitulate human nasal respiratory epithelium with ciliated cells, goblet cells, basal cells, club cells, and a thick mucus layer that is circulated by functional cilia and in contact with air.[25] Rajan *et al*. established HNOs as a model system for respiratory viral infections[25]; however, this model has not been previously applied to host-bacterial interactions.

HNOs overcome crucial limitations of other model systems for investigating epithelial-microbiont interactions. Primary human nasal epithelial cell explants (pHNECs), although physiologically equivalent, are restricted to short-term studies due to limited passaging.[26] Immortalized respiratory cell lines (e.g., CALU3, RPMI 2650, A549 cells) lack a physiological mucus layer, lack the multiple cell types present in human nasal epithelium, and fail to represent human genetic diversity.[27,28] ALI-polarization of these cell lines[29-31] or of immortalized human nasal epithelial cells[32] generates models that can tolerate live bacterial colonization for 4 to 72 hours, depending on the species[29-32]; however, these still fall short of recapitulating the human nasal mucociliary blanket. Animal models, e.g., the cotton rat[33], have the advantage of a systemic immune response; however, many human nasal microbionts poorly colonize nonhuman models and animal models of human nasal microbiota may nominally reflect human-microbe interactions.[34] As shown below, HNOs overcome these limitations.

Fixing HNOs in Clark's solution[35,36] and staining with Periodic acid-Schiff (PAS) and hematoxylin revealed a substantial apical mucus layer atop the epithelium with visible

apical ciliated cells, goblet cells, and numerous basal cells (**Figure 1A**). This robust mucus production by HNOs differentiated at ALI is a vital element since mucus affects bacterial behavior by reducing adherence and biofilm formation.[37,38] To replicate *in vivo* environmental conditions, we performed experiments with HNOs at the human nasal passage temperature of 34 °C.[39] Accounting for human nasal temperature is particularly important since *S. aureus*[31,40-42] and *S. pneumoniae*[43,44] behave differently at 34 °C, or lower, compared to at the human internal body temperature of 37 °C. Based on bulk RNA sequencing, HNOs differentiated at 37 °C and shifted to 34 °C for experimentation were transcriptionally similar to those maintained at 37 °C throughout (**Figure S1A**), indicating the shift to 34 °C had minimal effects on epithelial transcription. Hypothesizing that we could use these HNOs to investigate bacterial nasal colonization, we developed protocols for live bacterial monocolonization by *S. aureus*, *S. pneumoniae,* and *D. pigrum*.

All three nasal microbionts monocolonized HNOs at 34 °C, as measured by colony forming units (CFUs) recovered per HNO at 24 and 48 hours (**Figure 1B**). To preserve the mucus layer and maintain the air interface, we apically inoculated HNOs with 10^7 - 10^8 CFUs of bacteria in only 15 µL of buffer, with control HNOs receiving buffer alone (Methods in Supplemental Information). To account for host genetic variability, we used three different donor-derived HNO lines, which are indicated by different shapes in graphs. We used a linear mixed model (LMM) to account for the hierarchical nature of our data, with $n \geq 3$ independent experiments within each HNO line. The LMM allowed us to assess the variability due to both HNO line and independent experiments (as random effects). The variability due to HNO line was minimal when modeling the CFU and LDH data (**Table S1A-B**), allowing us to focus the model on the different bacterial treatments

(as a fixed effect). (For details on statistical analysis see reproducible code available at (https://klemonlab.github.io/HNOBac_Manuscript/).

All 3 HNO donor lines had a median of 6 x 10^5 human cells per transwell (**Figure S1B**) 1 day prior to bacterial inoculation for an estimated mean multiplicity of inoculation of 15 - 200. At 24 hours, *S. aureus* CFUs/HNO were reduced 374-fold from the inoculum, with an LMM-predicted mean of ~2.8 x 10^4 (**Table S1A**), but then appeared to rebound, increasing 330-fold between 24 and 48 hours (purple, **Figure 1B**), suggesting replication on the mucosal surface. At 24 hours, *D. pigrum* CFUs/HNO were reduced 990-fold from the inoculum, with a model-predicted mean of ~5.4 x 10^4 CFUs/HNO, which further decreased 17-fold by 48 hours (blue, **Figure 1B**). At 24 hours of colonization, *S. pneumoniae* CFUs/HNO were reduced 35-fold from the inoculum, with a model-predicted mean of ~10^6 CFUs/HNO, which further decreased 39-fold by 48 hours (lavender, **Figure 1B**). Experiments at human internal body temperature of 37 °C gave similar results (**Figure S1C**). Together, these assays demonstrate persistence of close to 10^5 CFUs/HNO at 24 or 48 hours, providing theoretically sufficient bacterial biomass for downstream assays in future experimentation. Moreover, these data point to the ability of the nasal epithelium to control the bacterial biomass during colonization.

Bacteria resided in the mucus layer during colonization. To assess bacterial localization, we colonized with live bacteria that were prelabeled with MitoTracker Red CMXRos[45] (which stains live bacterial cells and has fluorescence that survives fixation). Then, after HNO fixation and sectioning, we visualized the mucus layer and goblet cells using an anti-MUC5AC antibody and the epithelial cell nuclei and bacterial DNA using Hoechst 33342 dye (**Figure 1C-E**). Both colonized HNOs and uncolonized controls (**Figure 1F**) showed

secretion of MUC5AC+ mucus. Moreover, bacteria were visible in the mucus layer of HNOs after 6 hours of colonization (**Figure 1C-E**). This supports prior reports of *S. aureus* localization in mucus during nasal colonization of ferrets[46] and of *S. pneumoniae* localization in mucus layer during colonization of nasal epithelial tissue explants.[47]

To assess HNO health following bacterial colonization, we measured lactate dehydrogenase (LDH), an enzyme that is released from epithelial cells when plasma membrane integrity is compromised, in the basal medium.[48] For uncolonized HNOs, LDH levels in the basal medium increased 1.6-fold between 1 hour before colonization to 48 hours (**Figure 1G**). HNOs colonized with *D. pigrum* or *S. pneumoniae* released similar amounts of LDH as uncolonized controls (**Figure 1G, Table S1B**). HNO colonized with *S. aureus* released slightly (3.5-fold) more LDH by 48 hours than did uncolonized controls (**Figure 1G, Table S1B**). Similar results were obtained at 37 °C (**Figure S1D**). These data indicate a similarly low level of cellular damage in uncolonized and bacterially colonized HNOs.

HNOs displayed both species-specific and general cytokine production in response to monocolonization with *S. aureus*, *D. pigrum*, or *S. pneumoniae*. Based on their pathogenic potential, we hypothesized the pathobionts *S. aureus* and *S. pneumoniae* would initiate a more prominent nasal epithelial innate immune response compared to the candidate mutualist *D. pigrum*. To test this, we measured HNO apical and basal cytokine production in response to monocolonization with each species, with apical production modeling release into human nasal mucus/lumen and basal production modeling release into tissue and circulation. We assayed a wide range of epithelial-produced cytokines (including those involved in allergic response, inflammasome signaling, matrix

metalloproteinases, acute inflammation, chemotaxis, growth factors, response to viral/bacterial infection, and anti-inflammation), totaling 39 cytokines, 30 of which met the threshold for detection in at least one compartment (apical and/or basal). To assess whether live and dead bacteria elicited similar effects, we also inoculated HNOs with a comparable number of dead bacteria killed by gamma irradiation, which should preserve the structure of surface-exposed antigens.[49] We visualized the $\log_2$-fold-change in each cytokine detected at 48 hours in each colonized condition vs. the uncolonized control HNO, which revealed both species-specific and general responses to bacterial colonization (**Figure S2A; Table S1C**).

In terms of a species-specific effect, *S. aureus* colonization induced interleukin-1 (IL-1) family cytokines consistent with an inflammasome response (**Figure 2A**). Inflammasomes are cytosolic multiprotein complexes that are assembled in response to pathogen-associated molecular patterns (PAMPs) and/or damage-associated molecular patterns (DAMPs). Inflammasomes serve as both sensors and effectors of downstream inflammatory responses usually leading to pyroptotic cell death, which releases intracellular defenses[50] and DAMPs that enhance recruitment of immune cells to the site of infection.[51] Monocolonization with live *S. aureus* increased release of interleukin-1 alpha (IL-1α) by 39-fold apically and 33-fold basally compared to uncolonized HNOs (**Figure 2A**). Again, we used an LMM for analysis, which showed that HNO line accounted for little of the variability (**Table S1D**). The fold changes mentioned here are based on the LMM predicted means (**Table S1E**). IL-1α is a key alarmin initiating inflammasome signaling.[52] Both the pro- and mature forms of IL-1α bind to and actively signal through the IL-1 receptor (IL-1R)[53], and the Luminex assay used here detects both forms. In

opposition, IL-1 receptor antagonist (IL-1RN, previously known as IL-1RA) competitively binds to the IL-1R inhibiting both the pro- and mature forms of IL-1α and dampening inflammasome activation. Live *S. aureus* monocolonization also increased HNO production of IL-1RN by 4-fold apically and 50-fold basally. This raised the question of whether IL-1α or IL-1RN is dominant in the HNO response to *S. aureus* colonization. Using the same samples, we detected net IL-1R activation in the HEK-Blue IL-1R reporter line indicating that IL-1α activity dominated apically (**Figure S2B**) and basally (**Figure S2C**) during live *S. aureus* colonization. Cells undergoing stress or damage release IL-1α, leading to inflammasome activation and subsequent release of mature IL-18 and/or IL-1β.[52] In response to live *S. aureus* colonization, HNOs also released higher levels of IL-18 (but not IL-1β) with a 23-fold apical and basal increase, suggesting inflammasome activation in a subset of epithelial cells in line with a very modest increase in LDH release under this condition (**Figure 1G**). In contrast, gamma-irradiated dead *S. aureus* had no effect on HNO production of IL-1 family cytokines compared to uncolonized (**Figure 2A**). Moreover, only live *S. aureus* increased apical IL-18 release and only live *S. aureus* increased basal HNO release of IL-1 family cytokines, with no detectable effect of live or dead *D. pigrum* or *S. pneumoniae*. In a human study of nasal inoculation with autologous *S. aureus*, increased IL-1β in nasal secretions was associated with *S. aureus* clearance from the nasal passage (IL-1α and IL-18 were not measured).[54] Thus, our data showing HNO release of IL-1 family cytokines in response to live *S. aureus* colonization recapitulates an *in vivo S. aureus* human nasal colonization response further supporting HNOs as a surrogate to identify host factors affecting *S. aureus* nasal colonization.

Several monocolonization conditions resulted in decreased secretion of cytokines involved in antimicrobial immune responses below the levels of uncolonized controls (**Figure 2B**). Live or dead *D. pigrum* or live *S. aureus* decreased apical production of CXCL10 (previously known as IP-10) ~10-fold compared to uncolonized control HNOs, whereas there was little-to-no apical change in response to *S. pneumoniae* (**Figure 2B**). CXCL10 binds to the CXCR3 receptor inducing many downstream functions, e.g., chemotaxis of CXCR3+ cells, regulation of cell growth and proliferation, and promotion of apoptosis.[55] CXCL10 also exhibits antibacterial effects against USA300 *S. aureus*[56] and can stimulate release of *S. aureus* Protein A.[57] CXCL10 promotes inflammation, which can have detrimental or beneficial effects on disease outcomes. For example, in adults, higher serum levels of CXCL10 are associated with increased severity of SARS-CoV2 infection[58] and higher levels of CXCL10 in nasal lavage fluid are associated with type 1 chronic rhinosinusitis.[59] In contrast, in infants, higher levels of CXCL10 in nasal washes are associated with protection against severe respiratory syncytial virus infection.[60] In young adults and children, nasal microbiota profiles enriched for *Dolosigranulum*/*Corynebacterium* are associated with lower likelihood of severe respiratory symptoms during SARS-CoV2 infections.[61] It is interesting to speculate that *D. pigrum* could modulate CXCL10 levels during SARS-CoV2 infection since high levels of CXCL10 in SARS-CoV2 infection are associated with increased severity.[58] Either live or dead *D. pigrum* suppressed nasal epithelial production of CXCL10, whereas only live, but not dead, *S. aureus* suppressed CXCL10 production (**Figure 2B**), suggesting different mechanisms of suppression. Although inoculating peripheral blood mononuclear cells with *S. aureus* peptidoglycan lowers CXCL10 protein levels[62], the nasal epithelial

response observed here required live *S. aureus*. In contrast, dead *S. pneumoniae* increased production of basal CXCL10 and apical CXCL11. Increased mucosal CXCL10 levels are associated with pneumococcal carriage in older adults.[63] CXCL11 also acts via binding to the CXCR3 receptor, activating the same pathways as CXCL10[64], and, along with CXCL10, is up-regulated in response to pneumococcal lung infection in mice.[65] Overall, our data demonstrate that the HNOs are an excellent model for investigating nasal epithelial cytokine responses to bacterial colonization.

HNOs also displayed some general responses to bacterial colonization. For example, in response to live or dead bacteria, HNOs increased production of cytokines that interact with macrophages and neutrophils (**Figure 2C**). Compared to uncolonized HNOs, both live and dead bacteria of all three species induced a 10-to-109-fold increase in apical and basal production of G-CSF and CCL20 (previously known as MIP-3α), except that dead *S. aureus* only induced a 3.4-fold increase in basal CCL20. CCL20 is a chemokine that attracts lymphocytes[66] and dendritic cells.[67] G-CSF is a growth factor that modulates neutrophil activity and enhances their survival in the epithelium.[68] In contrast to the increase in G-CSF and CCL20, bacterial colonization of HNOs induced only mild increases in the pleiotropic cytokines TNF and IL-6, e.g., live *D. pigrum* and *S. pneumoniae* induced a 5-to-6-fold increase in apical TNF (**Figure 2D**). Although, dead *S. pneumoniae* induced a 28- and 18-fold increase in IL-6 apical and basal, respectively. This finding is in line with observations of *S. aureus* cell-free conditioned medium on pHNECs[69] or bacteria colonization on immortalized cell lines.[30,70] In contrast to the low-level baseline production of TNF and IL-6, uncolonized HNOs produced high levels of IL-8 (ranging from 1,000 to 5,000 pg/mL) without an increase in response to bacterial

colonization. Of note, monocolonized HNOs did not increase production of type 1 interferons (**Figure S2A; Table 1**), a key epithelial response to bacterial and viral infection[71,72], consistent with this being a model of microbiont colonization of the human nasal epithelium.

To our knowledge, this is the first report using HNOs differentiated at an ALI to investigate colonization of nasal respiratory epithelium by human nasal microbionts. HNOs differentiated at ALI (2D) have been used previously to investigate disease phenotypes, e.g., cystic fibrosis[73] and chronic rhinosinusitis[74], as well as respiratory viral infections.[25,75] The differentiation at and maintenance of an ALI separates these HNOs from 3D HNOs and 2D HNOs with apical medium.[74,76-78] This study is also the first to show that colonizing bacteria restricted to the mucociliary blanket are sufficient to induce an innate immune response in nasal epithelium. Our results show that monocolonization of human nasal epithelium with three nasal species resulted in distinct colonization dynamics and host responses. An epidemic USA300 strain of MRSA showed an initial drop in mucosal burden followed by a subsequent rebound suggesting active replication on nasal epithelium. Moreover, the epithelial innate immune response to *S. aureus* included higher levels of IL-1 family cytokines, indicative of activation of an inflammasome response. Additionally, we demonstrated that the candidate nasal mutualist *D. pigrum* reduced human nasal epithelial production of CXCL10, an inflammatory cytokine implicated in antimicrobial response and immune activation. Nasal colonization by *D. pigrum* has repeatedly been associated with positive health outcomes and HNOs now provide a means to elucidate the mechanisms of *D. pigrum* interactions with human nasal epithelium. In contrast, *S. pneumoniae*, a nasal pathobiont associated with negative

health outcomes and worsened viral infection symptoms, increased HNO production of antimicrobial and inflammation-associated cytokines. Unlike experimental human pneumococcal colonization, HNOs could be used to study colonization by a broader range and more virulent serotypes of *S. pneumoniae,* expanding efforts to identify key mechanisms of pneumococcal nasal colonization. Future applications for HNOs include extension to the pediatric nasal epithelium[75] and potential for genetic manipulation of organoid lines, as is done with human intestinal organoids.[79] Overall, the data presented here demonstrate that HNOs are a powerful model system for elucidating microbiont-epithelial interactions and providing new insights into the functions of human nasal microbiota.

Acknowledgements. We thank the donors who make HNOs possible. We thank Sue Crawford for performing gamma irradiation of bacteria; Victoria Poplaski for RNA extraction of uncolonized HNOs; Scott Chimileski for microscopy advice; Pamela Parsons for microscopy staining; Elina Mosa for assistance with microscopy imaging; Robert Britton, Anthony Maresso, members of the Respiratory Organoid Group and of the Lemon Lab for helpful discussions. This research was supported by funding from the National Institute of Allergy and Infectious Diseases of the National Institutes for Health (NIH) under award U19AI157981 (K.P.L., K.A.P., S.E.B.), U19AI144297 (S.E.B), and U19AI116497 (P.A.P., S.E.B.). Services from the Texas Medical Center Digestive Disease Center Functional Genomics and Microbiome Core (FGM) and Tissue Analysis & Molecular Imaging Core (TAMI) were supported in part by NIH grant P30DK056338. Biostatistics services from the Baylor College of Medicine (BCM) Biostatistics and Informatics Shared Advanced Technology Core were underwritten by institutional funds

from BCM. The BCM Integrated Microscopy Core is supported by the Center for Advanced Microscopy and Image Informatics (CAMII) with funding from NIH (DK56338, CA125123, ES030285), and CPRIT (RP150578, RP170719).

Author Contributions. Conceptualization: A.I.B., L.A.K., K.P.L. Methodology: A.I.B., L.A.K., I.F.E., H.T., S.G.H., A.K., A.R., K.A.P., P.A.P., S.E.B., J.M.L. Investigation: L.A.K., A.I.B., A.K. Resources: A.K., S.E.B. Data curation. I.F.E. Formal analysis. I.F.E., A.I.B., L.A.K., H.N.P., S.G.H. Validation. L.A.K., A.I.B., J.M.L. Visualization: A.I.B., L.A.K., I.F.E., S.G.H., H.N.P Writing – original draft: A.I.B., L.A.K., I.F.E., K.P.L. Writing – review & editing: L.A.K., A.I.B., I.F.E., K.P.L., K.A.P., S.G.H., A.K., H.T., H.N.P., A.R., J.M.L., P.A.P., S.E.B. Funding acquisition: K.P.L., S.E.B. Supervision: I.F.E., K.P.L.

Declaration of Interests. The authors declare no competing interests.

Supplemental Information.

Document S1. Methods and Figures S1-S2

Table S1. Excel file with results of linear mixed models

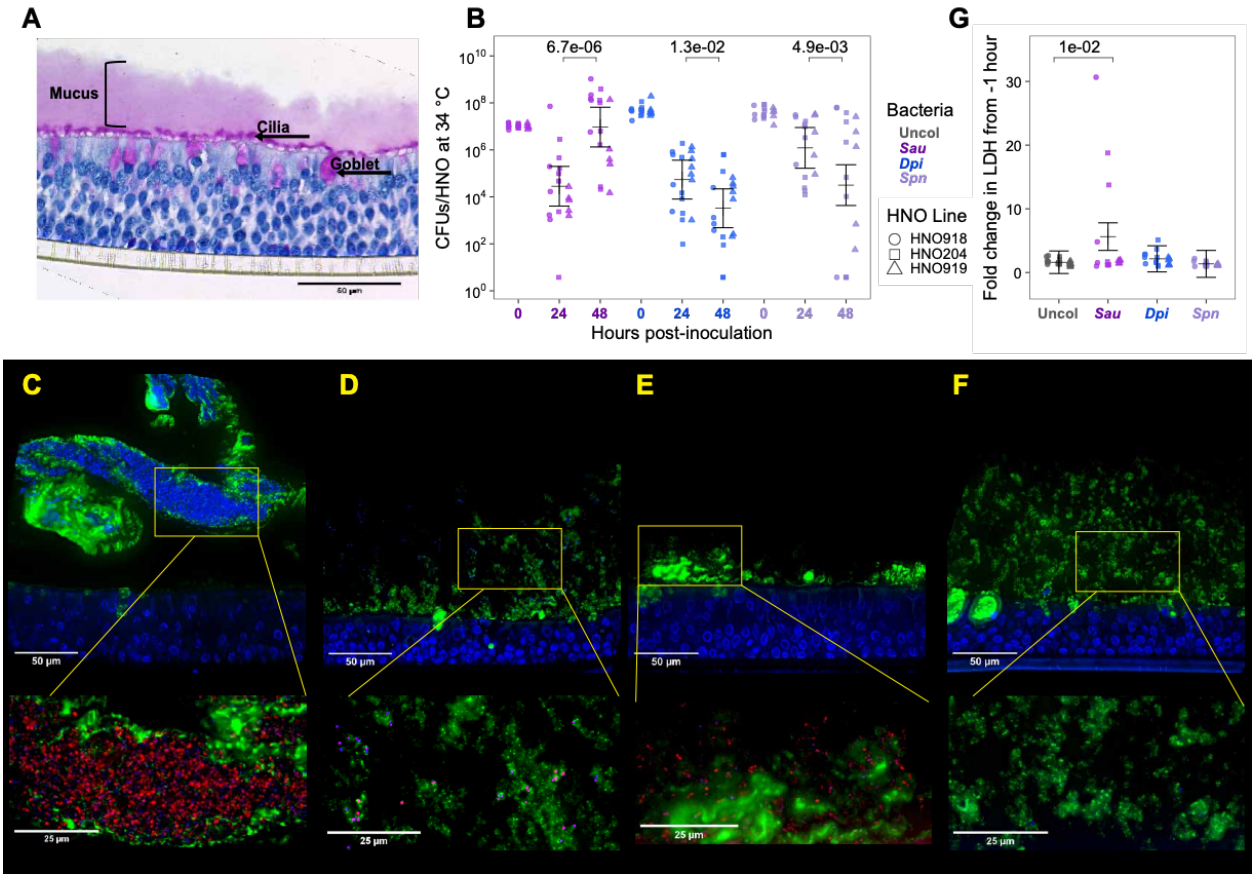

Figure 1. **Human nasal epithelial organoids tolerate nasal microbiont colonization and restrict bacteria to the mucus layer**. (**A**) HNOs differentiated at an ALI produced a robust mucus layer (pink). Uncolonized HNO919 was fixed in Clarke's solution, cross-sectioned, and stained with PAS (magenta) to highlight goblet cells, secreted mucus, and cilia, and with hematoxylin (navy) to highlight epithelial cells and imaged at 40x magnification. (**B**) Three HNO lines (HNO918 circles, HNO204 squares, HNO919 triangles) were each monocolonized with *S. aureus* (purple), *D. pigrum* (blue), and *S. pneumoniae* (lavender) at 34 °C for up to 48 h. At time 0, 10^7 CFUs of a bacterium in 15 µL of EBSS were inoculated apically. Recovered CFUs/HNO at 24 and 48 h are shown. Independent experiments for B, G: HNO918 ≥ 3, HNO204 ≥ 7, and HNO919 ≥ 5. Data (B and G) were analyzed using a linear mixed model (LMM) to determine statistical

significance with *p*-values adjusted for multiple comparisons (24 to 48 h in B and Uncolonized to each bacterial species in G) using the Holm method, shown above the horizontal bars. Vertical brackets represent the model-predicted mean values and confidence intervals (+/- twice the standard error of the mean). Including HNO line in the LMM as a random effect showed that HNO line accounted for little of the variability (**Table S1A-B**). (**C**) *D. pigrum,* (**D**) *S. aureus*, and (**E**) *S. pneumoniae* localized in the mucus layer at 6 h of HNO monocolonization. (**F**) Uncolonized HNO control. Shown are representative fluorescent images of cross-sections of colonized or uncolonized HNOs fixed and stained with anti-MUC5AC antibody highlighting mucus and goblet cells (green), and Hoechst highlighting host nuclei and bacterial cells (blue) at 60x magnification. Yellow boxes indicate the area that is shown below at a higher magnification (100x) to highlight bacteria (prestained with MitoTracker Red CMXRos prior to colonization) in the mucus layer. (**C**-**F**) Representative images are from experiments done with lines HNO204 and HNO918, each assayed on a different day: (**C**) HNO918, (**D**) HNO204, (**E**) HNO918, (**F**) HNO204. (**G**) Fold change in lactate dehydrogenase release of uncolonized (gray) HNOs, and HNOs colonized with *S. aureus* (purple), *D. pigrum* (blue), or *S. pneumoniae* (lavender) in HNO basal medium at 48 h compared to -1 h samples from the same well.

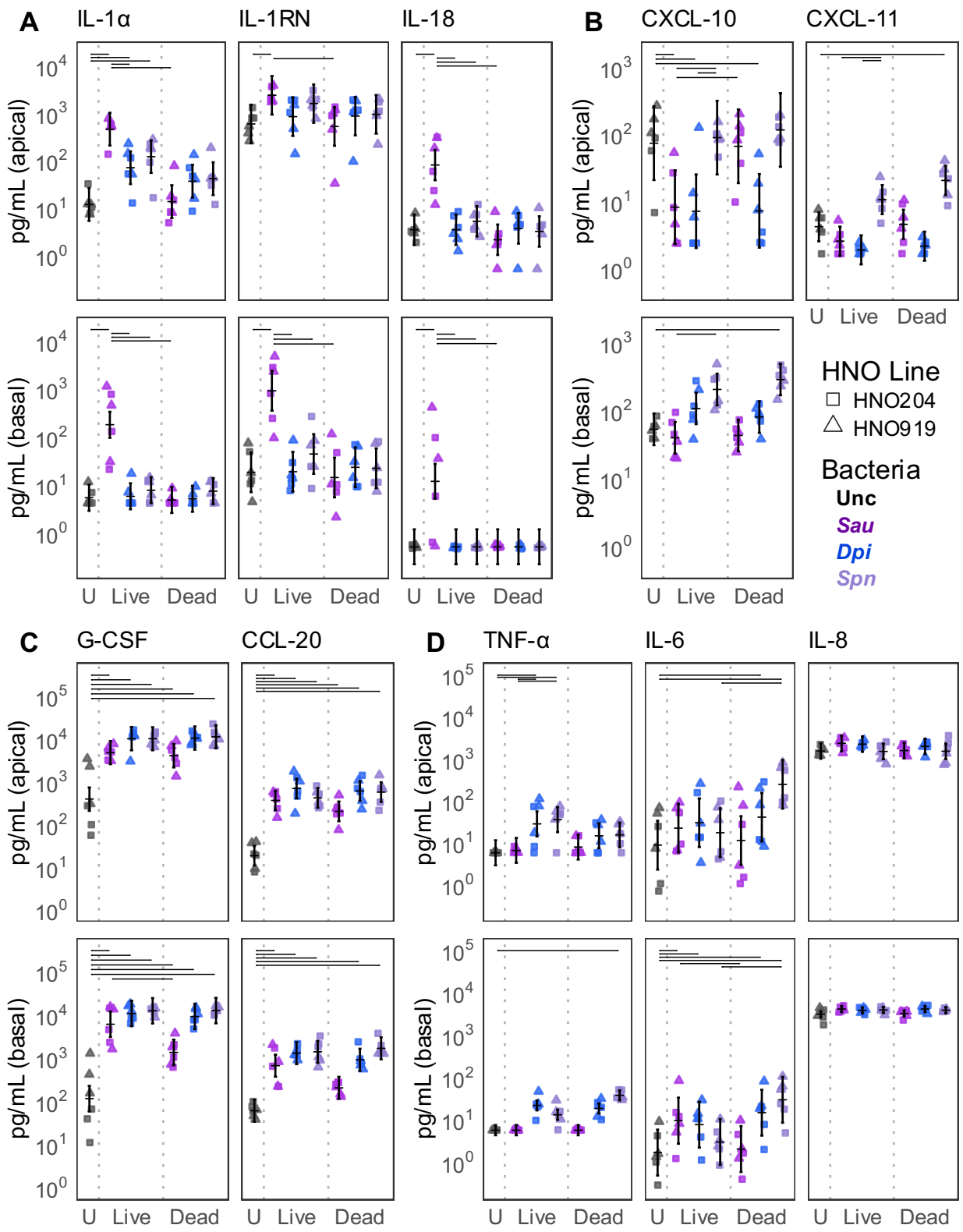
A
IL-1α
IL-1RN
IL-18
B
CXCL-10
CXCL-11
pg/mL (apical)
pg/mL (basal)
U Live Dead
HNO Line
HNO204
HNO919
Bacteria
Unc
Sau
Dpi
Spn
C
G-CSF
CCL-20
D
TNF-α
IL-6
IL-8

Figure 2. **Human nasal epithelium exhibits species-specific and general cytokine responses to colonization by common nasal microbionts**. HNO production of cytokines (pg/mL) detected in the apical wash or the basal medium after 48 h (shape indicates line and color indicates bacterial species). (Data for all 39 cytokines are in Table S1C-E with fold-change compared to the uncolonized control in Figure S2A). (**A**) Live *S. aureus* induced increased nasal epithelial production of IL-1 family cytokines (pg/mL) by 48 h, a response distinct from that to both *D. pigrum* and *S. pneumoniae*. (**B**) Live or dead *D. pigrum* and live *S. aureus* decreased epithelial apical production of CXCL10 compared to the uncolonized condition. In contrast, dead *S. pneumoniae* increased epithelial basal production of CXCL10 and apical production of CXCL11. (Basal CXCL11 was below limit of detection). (**C**) HNOs increased apical and basal production of G-CSF and CCL20 (MIP-3α) in response to all three bacteria, live or dead. (**D**) HNO production of TNF, IL-6, and IL-8 was modestly affected by bacterial monocolonization. Apical TNF mildly increased in response to live *D. pigrum* and *S. pneumoniae*, but not *S. aureus*. Apical IL-6 increased in response to dead *D. pigrum* or dead *S. pneumoniae.* Basal IL-6 increased in response to live *S. aureus*, live or dead *D. pigrum*, and dead *S. pneumoniae*. HNO production of IL-8 was stably high without and with bacterial colonization. Data are from three independent experiments in each of two HNO lines: HNO204 (squares), HNO919 (triangles). We used a linear mixed model to determine statistical significance. The vertical brackets represent the model-predicted mean values and confidence intervals (+/- twice the standard error of the mean). Horizontal lines are included connecting pairs of bacterial conditions for all analyzed contrasts that met the threshold for statistical significance (adjusted $p < 0.05$) and had a magnitude of effect greater than 4-fold (with

this threshold chosen to highlight differences with a larger effect size and improve readability of the bars). See **Table S1E** for all adjusted *p* values.

REFERENCES

1. Antimicrobial Resistance, C. (2022). Global burden of bacterial antimicrobial resistance in 2019: a systematic analysis. Lancet *399*, 629-655. 10.1016/S0140-6736(21)02724-0.
2. Kluytmans, J., van Belkum, A., and Verbrugh, H. (1997). Nasal carriage of *Staphylococcus aureus*: epidemiology, underlying mechanisms, and associated risks. Clinical microbiology reviews *10*, 505-520.
3. Gorwitz, R.J., Kruszon-Moran, D., McAllister, S.K., McQuillan, G., McDougal, L.K., Fosheim, G.E., Jensen, B.J., Killgore, G., Tenover, F.C., and Kuehnert, M.J. (2008). Changes in the prevalence of nasal colonization with *Staphylococcus aureus* in the United States, 2001-2004. J Infect Dis *197*, 1226-1234. 10.1086/533494.
4. von Eiff, C., Becker, K., Machka, K., Stammer, H., Peters, G., and Group, F.t.S. (2001). Nasal carriage as a source of *Staphylococcus aureus* bacteremia. N Engl J Med *344*, 11-16.
5. Wertheim, H.F., Vos, M.C., Ott, A., van Belkum, A., Voss, A., Kluytmans, J.A., van Keulen, P.H., Vandenbroucke-Grauls, C.M., Meester, M.H., and Verbrugh, H.A. (2004). Risk and outcome of nosocomial *Staphylococcus aureus* bacteraemia in nasal carriers versus non-carriers. Lancet *364*, 703-705. 10.1016/S0140-6736(04)16897-9.
6. Young, B.C., Wu, C.H., Gordon, N.C., Cole, K., Price, J.R., Liu, E., Sheppard, A.E., Perera, S., Charlesworth, J., Golubchik, T., et al. (2017). Severe infections emerge from commensal bacteria by adaptive evolution. Elife *6*. 10.7554/eLife.30637.
7. Missiakas, D., and Schneewind, O. (2016). Staphylococcus aureus vaccines: Deviating from the carol. J Exp Med *213*, 1645-1653. 10.1084/jem.20160569.
8. Miller, L.S., Fowler, V.G., Shukla, S.K., Rose, W.E., and Proctor, R.A. (2020). Development of a vaccine against Staphylococcus aureus invasive infections: Evidence based on human immunity, genetics and bacterial evasion mechanisms. FEMS Microbiol Rev *44*, 123-153. 10.1093/femsre/fuz030.
9. Bode, L.G., Kluytmans, J.A., Wertheim, H.F., Bogaers, D., Vandenbroucke-Grauls, C.M., Roosendaal, R., Troelstra, A., Box, A.T., Voss, A., van der Tweel, I., et al. (2010). Preventing surgical-site infections in nasal carriers of *Staphylococcus aureus*. N Engl J Med *362*, 9-17. 10.1056/NEJMoa0808939.
10. van Rijen, M., Bonten, M., Wenzel, R., and Kluytmans, J. (2008). Mupirocin ointment for preventing Staphylococcus aureus infections in nasal carriers. Cochrane Database Syst Rev, CD006216. 10.1002/14651858.CD006216.pub2.
11. Nair, R., Perencevich, E.N., Blevins, A.E., Goto, M., Nelson, R.E., and Schweizer, M.L. (2016). Clinical Effectiveness of Mupirocin for Preventing Staphylococcus aureus Infections in Nonsurgical Settings: A Meta-analysis. Clin Infect Dis *62*, 618-630. 10.1093/cid/civ901.
12. Richardson, E.J., Bacigalupe, R., Harrison, E.M., Weinert, L.A., Lycett, S., Vrieling, M., Robb, K., Hoskisson, P.A., Holden, M.T.G., Feil, E.J., et al. (2018). Gene exchange drives the ecological success of a multi-host bacterial pathogen. Nat Ecol Evol *2*, 1468-1478. 10.1038/s41559-018-0617-0.
13. WHO. One Health. https://www.who.int/health-topics/one-health#tab=tab_1.

14. Simell, B., Auranen, K., Kayhty, H., Goldblatt, D., Dagan, R., O'Brien, K.L., and Pneumococcal Carriage, G. (2012). The fundamental link between pneumococcal carriage and disease. Expert Rev Vaccines *11*, 841-855. 10.1586/erv.12.53.
15. CDC (2019). Antibiotic Resistance Threats in the United States, 2019.
16. Robinson, R.E., Myerscough, C., He, N., Hill, H., Shepherd, W.A., Gonzalez-Dias, P., Liatsikos, K., Latham, S., Fyles, F., Doherty, K., et al. (2023). Comprehensive review of safety in Experimental Human Pneumococcal Challenge. PLoS One *18*, e0284399. 10.1371/journal.pone.0284399.
17. Stubbendieck, R.M., Hurst, J.H., and Kelly, M.S. (2024). Dolosigranulum pigrum: A promising nasal probiotic candidate. PLoS Pathog *20*, e1011955. 10.1371/journal.ppat.1011955.
18. Escapa, I.F., Chen, T., Huang, Y., Gajare, P., Dewhirst, F.E., and Lemon, K.P. (2018). New Insights into Human Nostril Microbiome from the Expanded Human Oral Microbiome Database (eHOMD): a Resource for the Microbiome of the Human Aerodigestive Tract. mSystems *3*, e00187-00118. 10.1128/mSystems.00187-18.
19. Brugger, S.D., Eslami, S.M., Pettigrew, M.M., Escapa, I.F., Henke, M.T., Kong, Y., and Lemon, K.P. (2020). *Dolosigranulum pigrum* Cooperation and Competition in Human Nasal Microbiota. mSphere *5*, e00852-00820. 10.1128/mSphere.00852-20.
20. Liu, C.M., Price, L.B., Hungate, B.A., Abraham, A.G., Larsen, L.A., Christensen, K., Stegger, M., Skov, R., and Andersen, P.S. (2015). *Staphylococcus aureus* and the ecology of the nasal microbiome. Sci Adv *1*, e1400216. 10.1126/sciadv.1400216.
21. Laufer, A.S., Metlay, J.P., Gent, J.F., Fennie, K.P., Kong, Y., and Pettigrew, M.M. (2011). Microbial communities of the upper respiratory tract and otitis media in children. mBio *2*, e00245-00210. 10.1128/mBio.00245-10.
22. Bomar, L., Brugger, S.D., Yost, B.H., Davies, S.S., and Lemon, K.P. (2016). *Corynebacterium accolens* Releases Antipneumococcal Free Fatty Acids from Human Nostril and Skin Surface Triacylglycerols. mBio *7*, e01725-01715. 10.1128/mBio.01725-15.
23. De Boeck, I., Wittouck, S., Martens, K., Spacova, I., Cauwenberghs, E., Allonsius, C.N., Jorissen, J., Wuyts, S., Van Beeck, W., Dillen, J., et al. (2021). The nasal mutualist *Dolosigranulum pigrum* AMBR11 supports homeostasis via multiple mechanisms. iScience *24*, 102978. 10.1016/j.isci.2021.102978.
24. Sachs, N., Papaspyropoulos, A., Zomer-van Ommen, D.D., Heo, I., Bottinger, L., Klay, D., Weeber, F., Huelsz-Prince, G., Iakobachvili, N., Amatngalim, G.D., et al. (2019). Long-term expanding human airway organoids for disease modeling. EMBO J *38*. 10.15252/embj.2018100300.
25. Rajan, A., Weaver, A.M., Aloisio, G.M., Jelinski, J., Johnson, H.L., Venable, S.F., McBride, T., Aideyan, L., Piedra, F.A., Ye, X., et al. (2022). The Human Nose Organoid Respiratory Virus Model: an Ex Vivo Human Challenge Model To Study Respiratory Syncytial Virus (RSV) and Severe Acute Respiratory Syndrome Coronavirus 2 (SARS-CoV-2) Pathogenesis and Evaluate Therapeutics. mBio *13*, e0351121. 10.1128/mbio.03511-21.

26. Bukowy-Bieryllo, Z. (2021). Long-term differentiating primary human airway epithelial cell cultures: how far are we? Cell Commun Signal *19*, 63. 10.1186/s12964-021-00740-z.
27. Martens, K., Hellings, P.W., and Steelant, B. (2018). Calu-3 epithelial cells exhibit different immune and epithelial barrier responses from freshly isolated primary nasal epithelial cells in vitro. Clin Transl Allergy *8*, 40. 10.1186/s13601-018-0225-8.
28. Silva, S., Bicker, J., Falcao, A., and Fortuna, A. (2023). Air-liquid interface (ALI) impact on different respiratory cell cultures. Eur J Pharm Biopharm *184*, 62-82. 10.1016/j.ejpb.2023.01.013.
29. Kiedrowski, M.R., Paharik, A.E., Ackermann, L.W., Shelton, A.U., Singh, S.B., Starner, T.D., and Horswill, A.R. (2016). Development of an in vitro colonization model to investigate *Staphylococcus aureus* interactions with airway epithelia. Cell Microbiol *18*, 720-732. 10.1111/cmi.12543.
30. De Rudder, C., Calatayud Arroyo, M., Lebeer, S., and Van de Wiele, T. (2020). Dual and Triple Epithelial Coculture Model Systems with Donor-Derived Microbiota and THP-1 Macrophages To Mimic Host-Microbe Interactions in the Human Sinonasal Cavities. mSphere *5*. 10.1128/mSphere.00916-19.
31. Huffines, J.T., Boone, R.L., and Kiedrowski, M.R. (2024). Temperature influences commensal-pathogen dynamics in a nasal epithelial cell co-culture model. mSphere *9*, e0058923. 10.1128/msphere.00589-23.
32. Charles, D.D., Fisher, J.R., Hoskinson, S.M., Medina-Colorado, A.A., Shen, Y.C., Chaaban, M.R., Widen, S.G., Eaves-Pyles, T.D., Maxwell, C.A., Miller, A.L., et al. (2019). Development of a Novel ex vivo Nasal Epithelial Cell Model Supporting Colonization With Human Nasal Microbiota. Front Cell Infect Microbiol *9*, 165. 10.3389/fcimb.2019.00165.
33. Kokai-Kun, J.F., Walsh, S.M., Chanturiya, T., and Mond, J.J. (2003). Lysostaphin cream eradicates Staphylococcus aureus nasal colonization in a cotton rat model. Antimicrob Agents Chemother *47*, 1589-1597. 10.1128/AAC.47.5.1589-1597.2003.
34. Papazian, D., Wurtzen, P.A., and Hansen, S.W. (2016). Polarized Airway Epithelial Models for Immunological Co-Culture Studies. Int Arch Allergy Immunol *170*, 1-21. 10.1159/000445833.
35. Rajan, A., Robertson, M.J., Carter, H.E., Poole, N.M., Clark, J.R., Green, S.I., Criss, Z.K., Zhao, B., Karandikar, U., Xing, Y., et al. (2020). Enteroaggregative E. coli Adherence to Human Heparan Sulfate Proteoglycans Drives Segment and Host Specific Responses to Infection. PLoS Pathog *16*, e1008851. 10.1371/journal.ppat.1008851.
36. Green, S.I., Gu Liu, C., Yu, X., Gibson, S., Salmen, W., Rajan, A., Carter, H.E., Clark, J.R., Song, X., Ramig, R.F., et al. (2021). Targeting of Mammalian Glycans Enhances Phage Predation in the Gastrointestinal Tract. mBio *12*. 10.1128/mBio.03474-20.
37. Co, J.Y., Crouzier, T., and Ribbeck, K. (2015). Probing the Role of Mucin-Bound Glycans in Bacterial Repulsion by Mucin Coatings. Advanced Materials Interfaces *2*, 1500179. https://doi.org/10.1002/admi.201500179.

38. Fekete, E., and Buret, A.G. (2023). The role of mucin O-glycans in microbiota dysbiosis, intestinal homeostasis, and host-pathogen interactions. Am J Physiol Gastrointest Liver Physiol *324*, G452-G465. 10.1152/ajpgi.00261.2022.
39. Keck, T., Leiacker, R., Heinrich, A., Kuhnemann, S., and Rettinger, G. (2000). Humidity and temperature profile in the nasal cavity. Rhinology *38*, 167-171.
40. Bastock, R.A., Marino, E.C., Wiemels, R.E., Holzschu, D.L., Keogh, R.A., Zapf, R.L., Murphy, E.R., and Carroll, R.K. (2021). Staphylococcus aureus Responds to Physiologically Relevant Temperature Changes by Altering Its Global Transcript and Protein Profile. mSphere *6*. 10.1128/mSphere.01303-20.
41. Briaud, P., Frey, A., Marino, E.C., Bastock, R.A., Zielinski, R.E., Wiemels, R.E., Keogh, R.A., Murphy, E.R., Shaw, L.N., and Carroll, R.K. (2021). Temperature Influences the Composition and Cytotoxicity of Extracellular Vesicles in Staphylococcus aureus. mSphere *6*, e0067621. 10.1128/mSphere.00676-21.
42. Costa, F.G., Mills, K.B., Crosby, H.A., and Horswill, A.R. (2024). The Staphylococcus aureus regulatory program in a human skin-like environment. mBio *15*, e0045324. 10.1128/mbio.00453-24.
43. Gazioglu, O., Kareem, B.O., Afzal, M., Shafeeq, S., Kuipers, O.P., Ulijasz, A.T., Andrew, P.W., and Yesilkaya, H. (2021). Glutamate Dehydrogenase (GdhA) of Streptococcus pneumoniae Is Required for High Temperature Adaptation. Infect Immun *89*, e0040021. 10.1128/IAI.00400-21.
44. Basset, A., Herd, M., Daly, R., Dove, S.L., and Malley, R. (2017). The Pneumococcal Type 1 Pilus Genes Are Thermoregulated and Are Repressed by a Member of the Snf2 Protein Family. J Bacteriol *199*. 10.1128/JB.00078-17.
45. Vadia, S., Tse, J.L., Lucena, R., Yang, Z., Kellogg, D.R., Wang, J.D., and Levin, P.A. (2017). Fatty Acid Availability Sets Cell Envelope Capacity and Dictates Microbial Cell Size. Curr Biol *27*, 1757-1767 e1755. 10.1016/j.cub.2017.05.076.
46. Sanford, B.A., Thomas, V.L., and Ramsay, M.A. (1989). Binding of staphylococci to mucus in vivo and in vitro. Infect Immun *57*, 3735-3742. 10.1128/iai.57.12.3735-3742.1989.
47. Feldman, C., Read, R., Rutman, A., Jeffery, P.K., Brain, A., Lund, V., Mitchell, T.J., Andrew, P.W., Boulnois, G.J., Todd, H.C., and et al. (1992). The interaction of Streptococcus pneumoniae with intact human respiratory mucosa in vitro. Eur Respir J *5*, 576-583.
48. Riss, T., Niles, A., Moravec, R., Karassina, N., and Vidugiriene, J. (2004). Cytotoxicity Assays: In Vitro Methods to Measure Dead Cells. In Assay Guidance Manual, S. Markossian, A. Grossman, M. Arkin, D. Auld, C. Austin, J. Baell, K. Brimacombe, T.D.Y. Chung, N.P. Coussens, J.L. Dahlin, et al., eds.
49. Correa, W., Brandenburg, J., Behrends, J., Heinbockel, L., Reiling, N., Paulowski, L., Schwudke, D., Stephan, K., Martinez-de-Tejada, G., Brandenburg, K., and Gutsmann, T. (2019). Inactivation of Bacteria by gamma-Irradiation to Investigate the Interaction with Antimicrobial Peptides. Biophys J *117*, 1805-1819. 10.1016/j.bpj.2019.10.012.
50. Jorgensen, I., Zhang, Y., Krantz, B.A., and Miao, E.A. (2016). Pyroptosis triggers pore-induced intracellular traps (PITs) that capture bacteria and lead to their clearance by efferocytosis. J Exp Med *213*, 2113-2128. 10.1084/jem.20151613.

51. Dai, Y., Zhou, J., and Shi, C. (2023). Inflammasome: structure, biological functions, and therapeutic targets. MedComm (2020) *4*, e391. 10.1002/mco2.391.
52. Di Paolo, N.C., and Shayakhmetov, D.M. (2016). Interleukin 1alpha and the inflammatory process. Nat Immunol *17*, 906-913. 10.1038/ni.3503.
53. Kim, B., Lee, Y., Kim, E., Kwak, A., Ryoo, S., Bae, S.H., Azam, T., Kim, S., and Dinarello, C.A. (2013). The Interleukin-1alpha Precursor is Biologically Active and is Likely a Key Alarmin in the IL-1 Family of Cytokines. Front Immunol *4*, 391. 10.3389/fimmu.2013.00391.
54. Cole, A.L., Muthukrishnan, G., Chong, C., Beavis, A., Eade, C.R., Wood, M.P., Deichen, M.G., and Cole, A.M. (2016). Host innate inflammatory factors and staphylococcal protein A influence the duration of human Staphylococcus aureus nasal carriage. Mucosal Immunol *9*, 1537-1548. 10.1038/mi.2016.2.
55. Liu, M., Guo, S., Hibbert, J.M., Jain, V., Singh, N., Wilson, N.O., and Stiles, J.K. (2011). CXCL10/IP-10 in infectious diseases pathogenesis and potential therapeutic implications. Cytokine Growth Factor Rev *22*, 121-130. 10.1016/j.cytogfr.2011.06.001.
56. Crawford, M.A., Ward, A.E., Gray, V., Bailer, P., Fisher, D.J., Kubicka, E., Cui, Z., Luo, Q., Gray, M.C., Criss, A.K., et al. (2023). Disparate Regions of the Human Chemokine CXCL10 Exhibit Broad-Spectrum Antimicrobial Activity against Biodefense and Antibiotic-Resistant Bacterial Pathogens. ACS Infect Dis *9*, 122-139. 10.1021/acsinfecdis.2c00456.
57. Yung, S.C., Parenti, D., and Murphy, P.M. (2011). Host chemokines bind to Staphylococcus aureus and stimulate protein A release. J Biol Chem *286*, 5069-5077. 10.1074/jbc.M110.195180.
58. Lore, N.I., De Lorenzo, R., Rancoita, P.M.V., Cugnata, F., Agresti, A., Benedetti, F., Bianchi, M.E., Bonini, C., Capobianco, A., Conte, C., et al. (2021). CXCL10 levels at hospital admission predict COVID-19 outcome: hierarchical assessment of 53 putative inflammatory biomarkers in an observational study. Mol Med *27*, 129. 10.1186/s10020-021-00390-4.
59. Klingler, A.I., Stevens, W.W., Tan, B.K., Peters, A.T., Poposki, J.A., Grammer, L.C., Welch, K.C., Smith, S.S., Conley, D.B., Kern, R.C., et al. (2021). Mechanisms and biomarkers of inflammatory endotypes in chronic rhinosinusitis without nasal polyps. J Allergy Clin Immunol *147*, 1306-1317. 10.1016/j.jaci.2020.11.037.
60. Nicholson, E.G., Schlegel, C., Garofalo, R.P., Mehta, R., Scheffler, M., Mei, M., and Piedra, P.A. (2016). Robust Cytokine and Chemokine Response in Nasopharyngeal Secretions: Association With Decreased Severity in Children With Physician Diagnosed Bronchiolitis. J Infect Dis *214*, 649-655. 10.1093/infdis/jiw191.
61. Hurst, J.H., McCumber, A.W., Aquino, J.N., Rodriguez, J., Heston, S.M., Lugo, D.J., Rotta, A.T., Turner, N.A., Pfeiffer, T.S., Gurley, T.C., et al. (2022). Age-Related Changes in the Nasopharyngeal Microbiome Are Associated With Severe Acute Respiratory Syndrome Coronavirus 2 (SARS-CoV-2) Infection and Symptoms Among Children, Adolescents, and Young Adults. Clin Infect Dis *75*, e928-e937. 10.1093/cid/ciac184.

62. Li, Z., Levast, B., and Madrenas, J. (2017). Staphylococcus aureus Downregulates IP-10 Production and Prevents Th1 Cell Recruitment. J Immunol *198*, 1865-1874. 10.4049/jimmunol.1601336.
63. Urban, B.C., Goncalves, A.N.A., Loukov, D., Passos, F.M., Reine, J., Gonzalez-Dias, P., Solorzano, C., Mitsi, E., Nikolaou, E., O'Connor, D., et al. (2024). Inflammation of the nasal mucosa is associated with susceptibility to experimental pneumococcal challenge in older adults. Mucosal Immunol. 10.1016/j.mucimm.2024.06.010.
64. Tokunaga, R., Zhang, W., Naseem, M., Puccini, A., Berger, M.D., Soni, S., McSkane, M., Baba, H., and Lenz, H.J. (2018). CXCL9, CXCL10, CXCL11/CXCR3 axis for immune activation - A target for novel cancer therapy. Cancer Treat Rev *63*, 40-47. 10.1016/j.ctrv.2017.11.007.
65. Seyoum, B., Yano, M., and Pirofski, L.A. (2011). The innate immune response to Streptococcus pneumoniae in the lung depends on serotype and host response. Vaccine *29*, 8002-8011. 10.1016/j.vaccine.2011.08.064.
66. Hieshima, K., Imai, T., Opdenakker, G., Van Damme, J., Kusuda, J., Tei, H., Sakaki, Y., Takatsuki, K., Miura, R., Yoshie, O., and Nomiyama, H. (1997). Molecular cloning of a novel human CC chemokine liver and activation-regulated chemokine (LARC) expressed in liver. Chemotactic activity for lymphocytes and gene localization on chromosome 2. J Biol Chem *272*, 5846-5853. 10.1074/jbc.272.9.5846.
67. Le Borgne, M., Etchart, N., Goubier, A., Lira, S.A., Sirard, J.C., van Rooijen, N., Caux, C., Ait-Yahia, S., Vicari, A., Kaiserlian, D., and Dubois, B. (2006). Dendritic cells rapidly recruited into epithelial tissues via CCR6/CCL20 are responsible for CD8+ T cell crosspriming in vivo. Immunity *24*, 191-201. 10.1016/j.immuni.2006.01.005.
68. Martin, K.R., Wong, H.L., Witko-Sarsat, V., and Wicks, I.P. (2021). G-CSF - A double edge sword in neutrophil mediated immunity. Semin Immunol *54*, 101516. 10.1016/j.smim.2021.101516.
69. Hu, H., Liu, S., Hon, K., Psaltis, A.J., Wormald, P.J., and Vreugde, S. (2023). Staphylococcal protein A modulates inflammation by inducing interferon signaling in human nasal epithelial cells. Inflamm Res *72*, 251-262. 10.1007/s00011-022-01656-1.
70. Cantero, D., Cooksley, C., Jardeleza, C., Bassiouni, A., Jones, D., Wormald, P.J., and Vreugde, S. (2013). A human nasal explant model to study Staphylococcus aureus biofilm in vitro. Int Forum Allergy Rhinol *3*, 556-562. 10.1002/alr.21146.
71. McNab, F., Mayer-Barber, K., Sher, A., Wack, A., and O'Garra, A. (2015). Type I interferons in infectious disease. Nat Rev Immunol *15*, 87-103. 10.1038/nri3787.
72. Kovarik, P., Castiglia, V., Ivin, M., and Ebner, F. (2016). Type I Interferons in Bacterial Infections: A Balancing Act. Front Immunol *7*, 652. 10.3389/fimmu.2016.00652.
73. Micoli, F., Romano, M.R., Carboni, F., Adamo, R., and Berti, F. (2023). Strengths and weaknesses of pneumococcal conjugate vaccines. Glycoconj J *40*, 135-148. 10.1007/s10719-023-10100-3.
74. Ramezanpour, M., Bolt, H., Hon, K., Shaghayegh, G., Rastin, H., Fenix, K.A., Psaltis Alkis, J., Wormald, P.J., and Vreugde, S. (2022). Characterization of human

nasal organoids from chronic rhinosinusitis patients. Biol Open *11*. 10.1242/bio.059267.

75. Aloisio, G.M., Nagaraj, D., Murray, A.M., Schultz, E.M., McBride, T., Aideyan, L., Nicholson, E.G., Henke, D., Ferlic-Stark, L., Rajan, A., et al. (2024). Pediatric human nose organoids demonstrate greater susceptibility, epithelial responses, and cytotoxicity than adults during RSV infection. bioRxiv. 10.1101/2024.02.01.578466.
76. Li, L., Jiao, L., Feng, D., Yuan, Y., Yang, X., Li, J., Jiang, D., Chen, H., Meng, Q., Chen, R., et al. (2024). Human apical-out nasal organoids reveal an essential role of matrix metalloproteinases in airway epithelial differentiation. Nat Commun *15*, 143. 10.1038/s41467-023-44488-1.
77. Amatngalim, G.D., Rodenburg, L.W., Aalbers, B.L., Raeven, H.H., Aarts, E.M., Sarhane, D., Spelier, S., Lefferts, J.W., Silva, I.A., Nijenhuis, W., et al. (2022). Measuring cystic fibrosis drug responses in organoids derived from 2D differentiated nasal epithelia. Life Sci Alliance *5*. 10.26508/lsa.202101320.
78. Chiu, M.C., Li, C., Liu, X., Song, W., Wan, Z., Yu, Y., Huang, J., Xiao, D., Chu, H., Cai, J.P., et al. (2022). Human Nasal Organoids Model SARS-CoV-2 Upper Respiratory Infection and Recapitulate the Differential Infectivity of Emerging Variants. mBio *13*, e0194422. 10.1128/mbio.01944-22.
79. Lin, S.C., Qu, L., Ettayebi, K., Crawford, S.E., Blutt, S.E., Robertson, M.J., Zeng, X.L., Tenge, V.R., Ayyar, B.V., Karandikar, U.C., et al. (2020). Human norovirus exhibits strain-specific sensitivity to host interferon pathways in human intestinal enteroids. Proc Natl Acad Sci U S A *117*, 23782-23793. 10.1073/pnas.2010834117.

Supplemental Materials

Methods

Isolation and passaging of 3D human nasal organoids (HNOs). The isolation and passaging of human nasal epithelial organoids (aka human nose organoids) and the lines used here are previously described.[1,2] HNOs were established for use and distribution by the Baylor College of Medicine (BCM) 3D Organoid Core under a protocol (H-46014) approved by the BCM Institutional Review Board and with donor informed consent. In brief, both a nasal wash and a midturbinate swab were collected into a 50 mL conical tube from each donor and placed on ice until centrifugation. The supernatant was mixed with 10 mL airway organoid (AO) medium (as described in[1] without penicillin and streptomycin) containing 0.5 mg/ml collagenase (Sigma-C9407), 250 ng/mL amphotericin B, and 10 ng/mL gentamicin on an orbital shaker at 4 °C for 30 to 60 minutes (min). Three hundred µL of fetal bovine serum (FBS, Fisher #FB129999102) was added to the suspension to inactivate the collagenase and the suspension was mildly sheared using a 1 mL pipette tip and filtered through a 100-µm cell strainer (VWR #76327-102). The suspension was then centrifuged at 400 x g for 5 min at 4 ºC (Eppendorf 5702R). Supernatant was discarded and the cell pellet was washed twice in 10 mL wash medium (as described in[1] without penicillin and streptomycin) and centrifuged at 400 x g for 5 min at 4 °C. Each nasal-cell pellet was resuspended in 30 µL of Corning Matrigel GFR Basement Membrane Matrix (Corning #356231), placed in a 24-well culture plate, and incubated at 37 °C, 5% CO_2 for 20 min to solidify. Upon completed gelation, 500 µL of AO medium was added to each well and plates were incubated in a humidified 37 °C, 5% CO_2 (Thermo Scientific Heracell Vios 160i). The medium was changed every 4 days. The

cells were passaged every 7 days. To passage, the 3D HNOs were washed with 0.5 nM Ethylenediaminetetraacetic acid (EDTA, Thermo Scientific J15694AE) in cold Phosphate Buffered Saline (PBS) and centrifuged at 300 x g for 5 min at 4 ºC. Each cell pellet was resuspended in 500 µL of 0.05% trypsin-EDTA (Gibco 25300120) then incubated at 37 °C in a 5% CO_2 incubator for 4 min to break up the cells. To neutralize trypsin, we added 1 mL of wash medium with 10% FBS and dispersed the cells by pipetting 50 times. The cells were then centrifuged for 5 min at 300 x g and resuspended in 30 µL Matrigel per HNO to be generated. Cells were then placed into wells on a cell culture plate, allowed to solidify, and incubated as described above.

Differentiation of HNOs as 2D cultures at an air-liquid interface. As previously published[1], after 7 days of propagation in AO medium, 3D HNOs were washed with 5 nM EDTA as above to disperse cells and then incubated for 5 min in 0.05% trypsin-EDTA. We then added 1 mL of wash medium with 10% FBS and dispersed the 3D HNOs into approximately single cells by mechanically pipetting 160 times with a P1000 tip. The single-cell suspension was filtered through a 40-µm VWR cell strainer (#76327-098), then centrifuged for 5 min at 400 x g at 4 °C. The cell pellet was resuspended in AO medium supplemented with 25 ng/mL Epidermal Growth Factor (EGF; Gibco #PMG8043) and 150 µL of the single-cell suspension was plated drop by drop on the center of the apical side of a cell-culture-coated transwell insert (Corning #3470) pretreated with 30 µg/mL of bovine Type I collagen (Gibco #A1064401). Then 600 µL of AO medium supplemented with 25 ng/mL EGF was added to the basal side of each transwell. (One 3D HNO well was used to seed one transwell.) HNOs were incubated at 37 °C in a humidified 5% CO_2 incubator for 4 days, then medium was removed from both the basal and the apical sides

and 600 µL of PneumaCult Airway Organoid Differentiation Medium (AODM; STEMCELL Technologies #05060) was added only to the basal side creating an air-liquid interface (ALI) culture. Basal medium was changed twice weekly while HNOs were differentiated at ALI for 21 days.

Transepithelial electrical resistance (TEER). The minimum TEER for each batch of HNOs used for experiments was 600 Ohms. The median TEER for each line was as follows: HNO204 1100 Ohms, HNO918 808 Ohms, HNO919 840 Ohms. (The range of the average TEER (for measured wells) per experiment was as follows: HNO204 655-1860 Ohms, HNO918 585-1080 Ohms, HNO919 715-1460 Ohms.) We measured the TEER of 1 (and sometimes 2) individual HNO per line per experiment immediately after receiving wells from the Baylor College of Medicine 3D Organoid Core, which was ~24 hours before bacterial inoculation. We added 100 µL of Earle's Balanced Salt Solution without calcium, magnesium, or phenol red (EBSS; Gibco 14155063) to the apical side of the selected HNO, placed the TEER meter probe (World Precision Instruments EVOM2 with STX2 electrodes) into the liquid in the transwell according to the methods in[3], and recorded the Ohms. After probe removal, cells were scraped off the transwell with a pipet tip, resuspended in 100 µL of EBSS, and transferred to a clean 1.5 mL microcentrifuge tube for mycoplasma testing. After testing TEER on an individual HNO well, we changed the basal medium of all the other HNO wells and placed the 24-transwell plate into a humidified 5% CO_2 incubator at the specified temp (34 °C or 37 °C).

Mycoplasma testing. A representative well on each transwell plate for each HNO line was confirmed to be negative for *Mycoplasma* prior to experimentation as described here. The microfuge tube containing the resuspended HNO that had been used to measure

TEER (above) was heated at 95 °C for 15 min to lyse HNO cells. From the same transwell, we collected the basal medium into a separate 1.5 mL microcentrifuge tube. Each tube was used in a separate PCR reaction with either the Biovision Mycoplasma PCR Detection kit or the Venor GeM Mycoplasma Detection kit, per manufacturer's protocol. Electrophoresis on the PCR reactions on a 1% TopVision agarose gel made with and ran in a 1X Tris Acetate EDTA (TAE) buffer followed by staining DNA with SYBR Safe (Invitrogen #S33102) was used to detect which samples were positive for *Mycoplasma*. Only transwell plates with a representative HNO negative for *Mycoplasma* were used for experiments.

Epithelial RNA extraction and sequencing. HNOs were plated at ALI and differentiated at 37 ºC for 21 days, as described above. On day 21, the 2D HNOs at ALI were either collected for RNA extraction (red in Figure S1A) or shifted to 34 ºC for two more days (grey in Figure S1A). RNA was extracted from 2 pooled HNOs for each line from each condition. HNO wells were first washed once with 2x PBS. The following steps were then completed using the QIAGEN RNeasy Mini kit per the manufacturer's instructions using the on-column DNase digestion and Qiashredder tubes. Briefly, we added 350 µL of RLT buffer with β-mercaptoethanol (BME; 10 µL BME per 1 mL RLT buffer) in the HNO well and mixed by pipetting then transferred the lysate into a QIAshredder column for centrifugation at 16000 x g for 2 min at room temperature (RT), discarding the QIAshredder column. We added 350 µL of freshly made 70% ethanol to the filtrate and mixed well by pipetting. The sample was then transferred to a RNeasy Mini spin column in a 2 mL collection tube and centrifuged at 16000 x g for 30 sec, discarding filtrate. After performing the On-Column DNase digestion step, we continued with RNA cleanup steps.

To elute RNA, we placed the RNeasy spin column in a 1.5 mL collection tube, added 40 µL RNase-free water directly to the spin column membrane and centrifuged for 2 min at 16000 x g. A Nanodrop 2000 (Thermo Fisher Scientific) was used to quantify the RNA. A 260/230 ratio of ≥ 2 was the threshold for use for RNA sequencing. Novogene performed the sequencing using non-directional poly-A library preparation and 20 million paired reads using their Illumina NovaSeq 6000 and X-Plus Sequencing Platform.

Analysis of RNAseq data. We used the FASTQC package v0.11.9 to inspect the quality of the raw sequence reads. We used TrimGalore v0.6.5 with the default settings to remove Illumina adapters and low-quality basepairs prior to aligning reads to human genome build GRCh38.98 using HiSAT2 v2.2.1.[4] We then used featureCounts to generate a count matrix from the aligned reads. The DeSeq2 package (v1.44.0)[5] was used to perform principal component analysis of the feature count data. Detailed code to analyze the RNAseq data and create the corresponding plot is available online (https://klemonlab.github.io/HNOBac_Manuscript/Methods_RNASeq.html).

Enumeration of cells per HNO. To separate the HNO from the transwell, we added 200 µL of 0.25% Trypsin-EDTA (Gibco #25200056) and incubated at 37°C in a humidified 5% CO_2 incubator for 10-15 min. We then gently pipetted up and down 3 times with a 200 µL pipet tip to help dislodge the cells and incubated for an additional 10-15 minutes. We then gently pipetted up and down at least 20 times to disperse into individual cells and collected the suspension in a 1.5 mL Eppendorf tube. An aliquot of the nasal epithelial cell suspension was mixed with equal parts Trypan blue. Viable cells were counted manually using a Levy Double Count Chamber hemocytometer (Andwin Scientific 15170208).

Detailed code to analyze the cells count data and create the corresponding plots is available online (https://klemonlab.github.io/HNOBac_Manuscript/Methods_MOC.html).

Bacterial growth conditions. *Dolosigranulum pigrum* strain KPL3065[7], the USA300 methicillin-resistant *Staphylococcus aureus* strain JE2[8], and *Streptococcus pneumoniae* strain 603[9] were each grown on BD BBL Columbia agar medium with 5% sheep's blood (BAP) at 34°C in a humidified 5% CO_2 incubator. We struck from a frozen 15% glycerol stock stored at -80 °C onto BAP for single colonies. After 36 hours of growth, 10-15 *D. pigrum* single colonies were picked up with one sterile cotton swab (Puritan #25806) and bacteria were spread as a small lawn on one sterile 47 mm diameter, 0.2-µm polycarbonate membrane (Millipore Sigma #GTTP04700) atop BAP. This was repeated for four more BAP plates. After 36 hours of growth, we collected *D. pigrum* from 3-4 membranes using a sterile cotton swab, then resuspended the cells in EBSS, and adjusted the optical density at 600 nm (OD_{600}) to yield ~$1x10^7$ CFUs per 15 µL (as described below). We struck MRSA JE2 from a frozen glycerol stock for single colonies on a sterile 47 mm, 0.2-µm polycarbonate membranes on BAP. After 14 hours of growth, 5-10 colonies of MRSA were picked up with a sterile swab, resuspended cells in EBSS, and the resuspension was normalized to an OD_{600} that would yield ~$1x10^7$ CFUs per 15 µL EBSS. We struck *S. pneumoniae* from a frozen glycerol stock for singles directly onto BAP. After 12 hours of growth, 10-15 colonies were picked up with a sterile cotton swab and swabbed as a lawn onto a sterile 47 mm, 0.2-micron polycarbonate membranes atop BAP, preparing 4 plates. After 14 hours of growth, we collected *S. pneumoniae* lawns from 4 membranes on each side of a sterile swab, resuspended cells in EBSS, and adjusted the OD_{600} to yield ~$1x10^7$ CFUs per 15 µL EBSS.

Calculation of the number of bacterial colony forming units in a given optical density. *D. pigrum* was grown for 36 hours, and *S. aureus* and *S. pneumoniae* were grown for 12-14 hours, as described above. For each species, 20 - 30 single colonies were resuspended in 2-3 mL of EBSS and the OD_{600} was measured. We then made a series of suspensions in EBSS with a range of OD_{600} values from 0.1 to 1.5 and performed serial dilutions of each of the suspensions. A drip-plate method was used to enumerate CFUs. We inoculated 20 µL from each dilution twice onto BAP, tilting the petri dish to allow the 20 µL to drip down the plate to facilitate the counting of colonies after growth. After counting colonies, we calculated the total CFUs per 15 µL of original suspension for each OD_{600} value and generated a standard curve to determine what OD_{600} would yield an HNO inoculum of 10^7 CFUs/15 µL EBSS for each species.

Bacterial colonization of HNOs and enumeration of bacterial CFUs. We gently pipetted 15 µL of each bacterial suspension (~$1x10^7$ CFUs) onto the surface of each corresponding HNO in a transwell. Uncolonized control HNOs received 15 µL of EBSS alone. The 24-well transwell plates were then centrifuged at 120 x g for 1 min at 25°C in an Eppendorf Centrifuge 5430 R to help absorb the bacterial suspension into the apical mucus layer. HNOs were then incubated at either 34°C or 37°C in a humidified 5% CO_2 incubator. We collected HNOs for bacterial CFU enumeration after 24 or 48 hours by first removing basal medium and adding 75 µL of 0.25% Trypsin-EDTA to the apical surface of each well and incubating at 37 °C for 15 min to lift the HNO from the transwell. Second, we added 75 µL of 0.025% Triton-X 100 (Thermo Scientific J66624.AE) to each well and then pipetted the mixture up and down 30 times to fully break up the epithelial cell layer. We then made serial dilutions to enumerate the total bacterial CFUs on each HNO. In a

small subset of the independent experiments, *S. aureus* destroyed the HNO epithelial cell layer and the data from such wells was excluded from further analysis. Detailed code to analyze the CFU data, perform statistical analysis, and create the corresponding plots is available online (https://klemonlab.github.io/HNOBac_Manuscript/Methods_CFUs.html).

Lactate Dehydrogenase (LDH) Assay. Basal medium was collected at -1 and 48 hours relative to time of colonization from all HNO wells, including uncolonized controls, and immediately stored at -80 °C. LDH activity was measured in duplicate using the Promega CytoTox Non-Radioactive Cytotoxicity Assay (#G1780), per the manufacturer's instructions. Cytotoxicity for each experiment was calculated as the fold change in LDH in basal medium from an HNO at 48 h compared to the same HNO at -1 hour relative to colonization, including for the uncolonized controls. Detailed code to analyze the LDH data, perform statistical analysis, and create the corresponding plots is available online (https://klemonlab.github.io/HNOBac_Manuscript/Methods_LDH.html).

Brightfield Microscopy. Uncolonized HNOs were inoculated with 15 µL of EBSS then incubated at 34 °C for 24 hours. After 24 hours, we fixed HNOs in Clarke's solution (75% ethanol and 25% glacial acetic acid) by removing each HNO-containing transwell from its plate and submerging it in 2 mL of RT fixative in the well of a 24-well plate for 30 min. After fixation, HNO transwells were rinsed twice by submersion in 100% anhydrous methanol at 4 °C for $\geq$ 30 min. We then cut the bottom membrane, on which the HNO sits, of each transwell from its plastic housing with a sterile scalpel and stored the HNO plus membrane at 4 °C in anhydrous methanol until submission to the TMC Digestive Disease Center Tissue Analysis & Molecular Imaging Core for paraffin embedding, sectioning, and staining. Sections were stained with Sigma-Aldrich Microscopy PAS

staining kit (#1.01646.0001), and then counterstained with hematoxylin (Epredia, #7211). Images were taken with a Nikon Eclipse Ci-L bright field microscope (Serial Number 702085) at 40x magnification. Fiji Is Just ImageJ (FIJI) was used to white-balance the image and add a scale bar.

Fluorescence Microscopy. HNOs were inoculated with ~$1x10^7$ CFUs of *D. pigrum*, *S. aureus*, or *S. pneumoniae* in 15 µl of EBSS or, as a control, with EBSS alone, as described above. Live bacterial resuspensions were prestained with MitoTracker Red CMXRos (Invitrogen #M7512) before colonization.[10] Briefly, each bacterium was resuspended in 10-15 mL EBSS to an OD_{600} of 1 prior to adding 1 µL of 1 mM MitoTracker Red CMXRos per mL of resuspension and incubating at RT for 1 hour. Prestained bacteria were washed twice with 10-15 mL of EBSS by centrifugation at 10000 x g for 10 min at RT and resuspended in EBSS. The OD_{600} of each resuspension was adjusted to yield ~$1x10^7$ CFUs per 15 µL EBSS and HNOs were monocolonized with bacteria as described above. After 6 h of colonization at 34 °C, we fixed HNOs, including uncolonized controls, in Clarke's solution, and stored them as described above. Samples were submitted to the TMC Digestive Disease Center Tissue Analysis & Molecular Imaging Core for paraffin embedding, sectioning, and staining. Briefly, after tissue processing, the membranes were bisected and embedded in paraffin (Richard-Allen Scientific, 22900700) for cross-sectioning. The paraffin-embedded membranes were deparaffinized and subjected to antigen retrieval (Biocare, CB910M). The sections were incubated with 4% bovine serum for 1 hour to block nonspecific protein binding, then were incubated overnight at 4°C with the primary antibody, MUC5AC (Invitrogen, #MA5-12178, dilution 1:1000). The MUC5AC primary was detected using an Alexa Fluor 488-conjugated goat

anti-mouse secondary antibody (Invitrogen #A11001; dilution 1:300), and the slides were counterstained with Hoechst (Invitrogen™ 33258 #H3569, dilution 1:10,000) for 10 min and washed with deionized (DI) water. Coverslips were added with Invitrogen ProLong Glass Antifade Mountant (#P36980). Stained HNOs were imaged using an Olympus IX83 epifluorescence deconvolution microscope (#2000 IXplore IX83) equipped with an IX3 laser (#IX3-ZDC2) at 60x magnification using the blue (excitation 350 +/- 25 nm, emission 460 +/- 25 nm) and green (excitation 470 +/- 20 nm, emission 525 +/- 25 nm) channels to detect the Hoechst and MUC5AC signal, respectively. Stained HNOs were imaged at 100x magnification using the blue, green, and red (excitation 560 +/- 20 nm, emission 630 +/- 37.5 nm) channels to detect the Hoechst, MUC5AC, and MitoTracker Red CMXRos signal, respectively. All images were processed for publication using FIJI to adjust contrast to maximize visibility and minimize overexposure in each color channel separately, merge channels, and add scale bars.

Gamma-irradiation to kill bacteria. To sufficiently inactivate bacteria while maintaining structural integrity, we irradiated each bacterium with between > 1,000 and < 8,000 grays, per Correa et al..[11] We resuspended each bacterial species separately in EBSS to an OD_{600} equal to ~$1x10^7$ CFUs/15 µL and added 25 mL of each bacterial resuspension separately to a 50 mL conical tube and irradiated overnight in a Gammacell-1000 Irradiator (Atomic Energy of Canada Ltd.) with a Cesium-137 source. This instrument generates 758.3 rads/min, and each sample was irradiated for ~9.5 hours for a total of 4,322 grays of radiation. After irradiation, we gently washed bacteria to remove lingering reactive oxygen species by pelleting cells at 6,000 x g for 10 min, removing the supernatant, and resuspending in an equal amount of EBSS. We plated 2 drips of 20 µL

of each resuspension on BAP and cultured for 48 hours at 34°C in a humidified 5% CO_2 incubator and verified the absence of viable bacteria. We aliquoted the remaining resuspension in 1 ml aliquots and flash-froze each in a dry ice and ethanol mix before storage at -80 °C. For each experiment, we thawed a fresh aliquot of gamma-irradiated bacteria at RT, and we used 15 µL of each resuspension to inoculate an HNO with dead bacteria. Two 20 µL drips were plated at the beginning of each experiment to verify the absence of viable bacteria in the experimental inoculum.

Immunoassays for detection of cytokines. HNOs were colonized with either live (approximately 10^7 CFUs) or dead (gamma-irradiated) bacteria resuspended in EBSS and included uncolonized control HNOs inoculated with buffer alone. After 48 hours at 34°C in a humidified CO_2 incubator, basal medium was collected from each well and transferred to a sterile 1.5 mL microcentrifuge tube. The apical side of each HNO was separately washed by adding 150 µL of AODM and pipetting up and down 3 times before transferring the wash to a sterile 1.5 mL microcentrifuge tube. Each HNO was washed a second time with the same volume and both washes were pooled. Samples were frozen at -80 °C until use in immunoassays. For immunoassays, samples were submitted to the Digestive Disease Center Functional Genomics and Microbiome core with the following Millipore Sigma magnetic-bead panel kits: 1) Milliplex Human Cytokine Panel III with IL-29, I-TAC, CCL20/MIP-3a, MIP-3b; 2) Milliplex Human Cytokine Panel A with MIG, IFNg, IFNa2, TNF-a, IP-10, RANTES, IL-1a, IL-1ra, IL-1b, IL-5, IL-6, IL-8, IL-10, IL-12p70, IL-13, IL-18, MIP-1a, MIP-1b, MCP-1, MCP-3, IL-17A, IL-17E/IL-25, Eotaxin/CCL11, G-CSF, GM-CSF, VEGF-A; 3) Milliplex Human MMP Panel 2 with MMP1, MMP2, MMP7, MMP9 and MMP10; and 4) Milliplex Human Cytokine Panel IV with IL-32, IL-36/IL-1F8,

IL-37/IL-1F7, IL-38/IL-1F10. Samples were assayed per the manufacturer's instructions and analyzed with Luminex xPONENT for Magpix (version 4.2, build 1324) on a Magpix instrument. Data was analyzed with Milliplex Analyst (version 5.1.0.0, standard build 10/27/2012). All sample values below the manufacturer's limit of detection were set at the limit of detection for analysis. Each individual assay of a cytokine at a given location (e.g., apical IL-6) was considered below the limit of detection (gray tiles in Figure S2A) if > 75% of the (39) samples were at or below the manufacturer's limit of detection, except when the few samples (≤ 25% of the total samples) above that threshold had $\log_2$-fold changes for colonized compared to uncolonized that were ≥ 2.5 times higher than samples at the limit of detection. This only occurred for basal production of IL-18 in response to live MRSA. Detailed code to analyze the cytokine data, perform statistical analysis, and create the corresponding plots is available online (https://klemonlab.github.io/HNOBac_Manuscript/Methods_Cytokines.html).

Detection of catalytically active IL-1α and IL-1β. HEK-Blue™ IL-1R Cells (InvivoGen **HKB-IL1R**) were propagated according to the manufacturer's instructions. These reporter cells detect both IL-1α and IL-1β activity, without distinction, to the extent that it is greater than IL-1RN activity. The same apical and basal medium samples used for cytokine detection were tested for catalytically active IL-1α and IL-1β. Briefly, after adding 20 µL of either HNO basal medium or apical wash to the bottom of a 96-well plate, we inoculated each well with 3×10^5 HEK-Blue cells and incubated for 22 hours at 37 °C in a humidified 5% CO_2 incubator. HEK-Blue cells partially adhere to the bottom of the 96-well plate during incubation. At collection, plates were tapped gently to mix the liquid and 20 µL of spent HEK medium from each well was transferred into a corresponding well of a new

96-well plate prior to addition of 180 µL of freshly prepared QUANTI-Blue™ Solution (Invivogen REPQBS) per well. The assay developed at 37 °C for 2.5 hours before reading absorbance at 620 nm. A standard curve was constructed using InvivoGen recombinant human IL-1β as a positive control. Detailed code to analyze the HEK-Blue data and create the corresponding plots is available online (https://klemonlab.github.io/HNOBac_Manuscript/Methods_HekBlue.html).

Statistical Analysis. R (v4.4.0) and RStudio (v2023.12.1+402) were used for data analysis, statistics, and data visualization[12,13]. A complete list of the R packages used is available at https://klemonlab.github.io/HNOBac_Manuscript/RSession.html. For analysis of the CFU, LDH, and cytokines data, we used the lme4 package (v1.1-35.5) to fit the data to linear mixed-effects models.[14] For each assayed HNO temperature, we modeled the log-transformed CFU counts (excluding initial inoculum measurements at time 0) considering bacterial species and collection timepoint as fixed effects. Likewise, at each HNO temperature, we modeled the ratio of LDH activity after 48 h of colonization relative to 1 h before colonization with bacterial species as a fixed effect. We modeled the log-transformed pg/mL data for each different cytokine assay derived from the apical or basal surfaces of the HNOs separately defining as fixed effect in each model the interaction variable "Bac.Via" that combines bacterial condition (uncolonized, *D. pigrum, S. aureus*, or *S. pneumoniae*) with viability status (control, live, or dead). Across all the analyzed data we considered experimental replicate (i.e., date) nested under HNO line as random effects (**Table S1E**). This identifies and corrects for the percentage of variation due to donor line differences and experimental batch effects. Some of the cytokine's fitted models were 'singular' due to HNO line-associated variance being close to zero; those

models were recalculated with only experimental replicate as a random effect. We performed an ANOVA for each model with *p*-values added by the afex package (v1.4-1).[15] If the resultant global *p*-value for fixed effects was < 0.05, then individual contrasts were calculated with the emmeans package (v1.10.4).[16] We used the Holm method[17] for multiple comparisons adjustment for comparing results from each bacterial species at the 24 and 48 h timepoints in the CFU data (3 contrasts) and to compare each species to the uncolonized condition in the LDH data (3 contrasts). For the cytokine data we analyzed the following contrasts: the uncolonized control and all other conditions, all combinations of live bacterial species, and live vs. dead for each bacterium. In view of the large number of comparisons (588 contrasts), to account for multiple comparisons, we then used FDR[18] for adjustment across all the selected contrasts across all cytokine assays (**Table S1D**). Detailed code for all statistical analysis is available online (https://klemonlab.github.io/HNOBac_Manuscript/index.html).

Data Availability. Sequencing data files and raw count matrix file are available at the Gene Expression Omnibus, accession number GSE277582.

REFERENCES

1. Rajan, A., Weaver, A.M., Aloisio, G.M., Jelinski, J., Johnson, H.L., Venable, S.F., McBride, T., Aideyan, L., Piedra, F.A., Ye, X., et al. (2022). The Human Nose Organoid Respiratory Virus Model: an Ex Vivo Human Challenge Model To Study Respiratory Syncytial Virus (RSV) and Severe Acute Respiratory Syndrome Coronavirus 2 (SARS-CoV-2) Pathogenesis and Evaluate Therapeutics. mBio *13*, e0351121. 10.1128/mbio.03511-21.
2. Aloisio, G.M., Nagaraj, D., Murray, A.M., Schultz, E.M., McBride, T., Aideyan, L., Nicholson, E.G., Henke, D., Ferlic-Stark, L., Rajan, A., et al. (2024). Pediatric human nose organoids demonstrate greater susceptibility, epithelial responses, and cytotoxicity than adults during RSV infection. bioRxiv. 10.1101/2024.02.01.578466.
3. Srinivasan, B., Kolli, A.R., Esch, M.B., Abaci, H.E., Shuler, M.L., and Hickman, J.J. (2015). TEER measurement techniques for in vitro barrier model systems. J Lab Autom *20*, 107-126. 10.1177/2211068214561025.
4. Liao, Y., Smyth, G.K., and Shi, W. (2014). featureCounts: an efficient general purpose program for assigning sequence reads to genomic features. Bioinformatics *30*, 923-930. 10.1093/bioinformatics/btt656.
5. Love, M.I., Huber, W., and Anders, S. (2014). Moderated estimation of fold change and dispersion for RNA-seq data with DESeq2. Genome Biol *15*, 550. 10.1186/s13059-014-0550-8.
6. Wickham, H., and Sievert, C. (2016). Ggplot2 : elegant graphics for data analysis, Second edition. Edition (Springer).
7. Flores Ramos, S., Brugger, S.D., Escapa, I.F., Skeete, C.A., Cotton, S.L., Eslami, S.M., Gao, W., Bomar, L., Tran, T.H., Jones, D.S., et al. (2021). Genomic Stability and Genetic Defense Systems in *Dolosigranulum pigrum*, a Candidate Beneficial Bacterium from the Human Microbiome. mSystems *6*, e0042521. 10.1128/mSystems.00425-21.
8. Fey, P.D., Endres, J.L., Yajjala, V.K., Widhelm, T.J., Boissy, R.J., Bose, J.L., and Bayles, K.W. (2013). A genetic resource for rapid and comprehensive phenotype screening of nonessential *Staphylococcus aureus* genes. mBio *4*, e00537-00512. 10.1128/mBio.00537-12.
9. Malley, R., Lipsitch, M., Stack, A., Saladino, R., Fleisher, G., Pelton, S., Thompson, C., Briles, D., and Anderson, P. (2001). Intranasal immunization with killed unencapsulated whole cells prevents colonization and invasive disease by capsulated pneumococci. Infect Immun *69*, 4870-4873. 10.1128/IAI.69.8.4870-4873.2001.
10. Vadia, S., Tse, J.L., Lucena, R., Yang, Z., Kellogg, D.R., Wang, J.D., and Levin, P.A. (2017). Fatty Acid Availability Sets Cell Envelope Capacity and Dictates Microbial Cell Size. Curr Biol *27*, 1757-1767 e1755. 10.1016/j.cub.2017.05.076.
11. Correa, W., Brandenburg, J., Behrends, J., Heinbockel, L., Reiling, N., Paulowski, L., Schwudke, D., Stephan, K., Martinez-de-Tejada, G., Brandenburg, K., and Gutsmann, T. (2019). Inactivation of Bacteria by gamma-Irradiation to Investigate the Interaction with Antimicrobial Peptides. Biophys J *117*, 1805-1819. 10.1016/j.bpj.2019.10.012.

12. R-Core-Team (2021). R: A Language and Environment for Statistical Computing (R Foundation for Statistical Computing).
13. RStudio-Team (2020). RStudio: Integrated Development for R. RStudio (PBC).
14. Bates, D., Mächler, M., Bolker, B., and Walker, S. (2015). Fitting Linear Mixed-Effects Models Using lme4. Journal of Statistical Software *67*, 1 - 48. 10.18637/jss.v067.i01.
15. Singmann, H., Bolker, B., Westfall, J., Aust, F., Ben-Shachar, M. S. (2024). afex: Analysis of Factorial Experiments.
16. Lenth, R.V. (2024). emmeans: Estimated Marginal Means, aka Least-Squares Means.
17. Holm, S. (1979). A Simple Sequentially Rejective Multiple Test Procedure. Scandinavian Journal of Statistics *6*, 65-70.
18. Benjamini, Y., and Hochberg, Y. (1995). Controlling the False Discovery Rate: A Practical and Powerful Approach to Multiple Testing. Journal of the Royal Statistical Society. Series B (Methodological) *57*, 289-300.

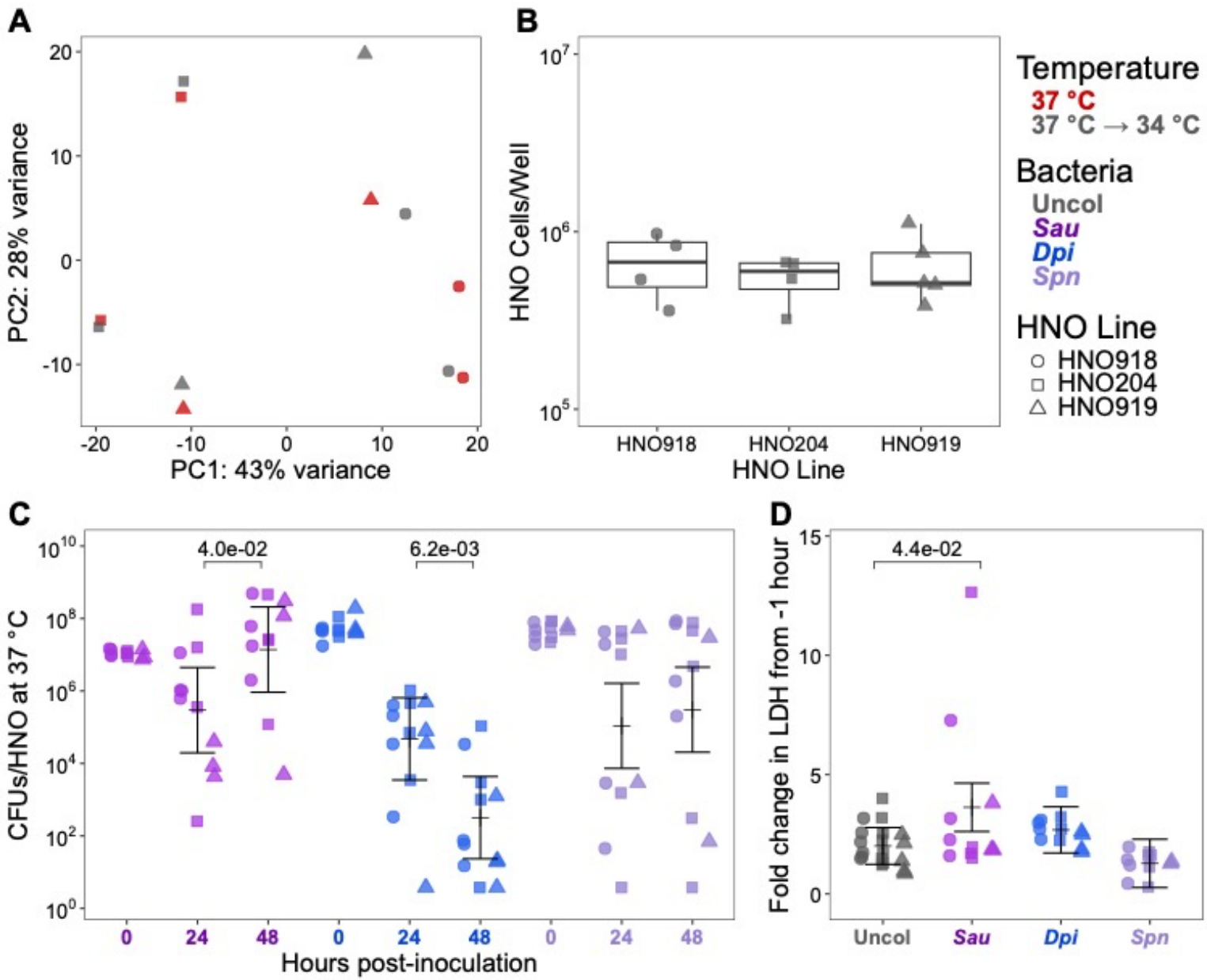
A
PC2: 28% variance
PC1: 43% variance
B
HNO Cells/Well
HNO918
HNO204
HNO919
HNO Line
Temperature
37 °C
37 °C → 34 °C
Bacteria
Uncol
Sau
Dpi
Spn
HNO Line
HNO918
HNO204
HNO919
C
CFUs/HNO at 37 °C
4.0e-02
6.2e-03
Hours post-inoculation
D
Fold change in LDH from -1 hour
4.4e-02
Uncol
Sau
Dpi
Spn

Figure S1. **Nasal microbionts colonize HNOs at human internal body temperature, 37 °C.** (**A**) In a Principal Component Analysis, epithelial transcription (read counts) within an HNO line was comparable between HNOs differentiated at 37 °C for 21 days (red) and HNOs shifted to 34 °C (gray) for an additional 2 days after the 21 days of differentiation at 37 °C (*n* = 2 independent experiments with 3 HNO lines). (**B**) HNO lines derived from different donors had comparable cells per HNO well. The median number of cells in each HNO was 6.01×10^5 for line HNO204, 6.9×10^5 for line HNO918, and 5.15×10^5 for line HNO919 in *n* = 4 independent experiments per line. (**C**) HNOs were monocolonized with *S. aureus* (purple), *D. pigrum* (blue), and *S. pneumoniae* (lavender) at 37 °C for up to 48 h. At time 0, 10^7 CFUs of a bacterium in 15 µL of EBSS were inoculated apically. Recovered CFUs/HNO at 24 and 48 h are shown. (**D**) Fold change in lactate dehydrogenase release of uncolonized (gray) HNOs, and HNOs colonized with *S. aureus* (purple), *D. pigrum* (blue), or *S. pneumoniae* (lavender) into HNO basal medium at 48 h compared to samples taken 1 h prior to colonization from the same well at 37 °C. HNOs colonized by *S. aureus* had 1.8-fold higher basal LDH release compared to the uncolonized control. For **C** and **D,** the independent experiments per HNO line were HNO918 $\geq$ 4, HNO204 $\geq$ 4, and HNO919 $\geq$ 2. Data (**C, D**) were analyzed using a linear mixed model to determine statistical significance and the Holm method was used to adjust *p*-values (shown above the horizontal bars) for multiple comparisons (24 to 48 h in C and uncolonized to each bacterial treatment in D). Vertical brackets represent the model-predicted mean values and confidence intervals (+/- twice the standard error of the mean).

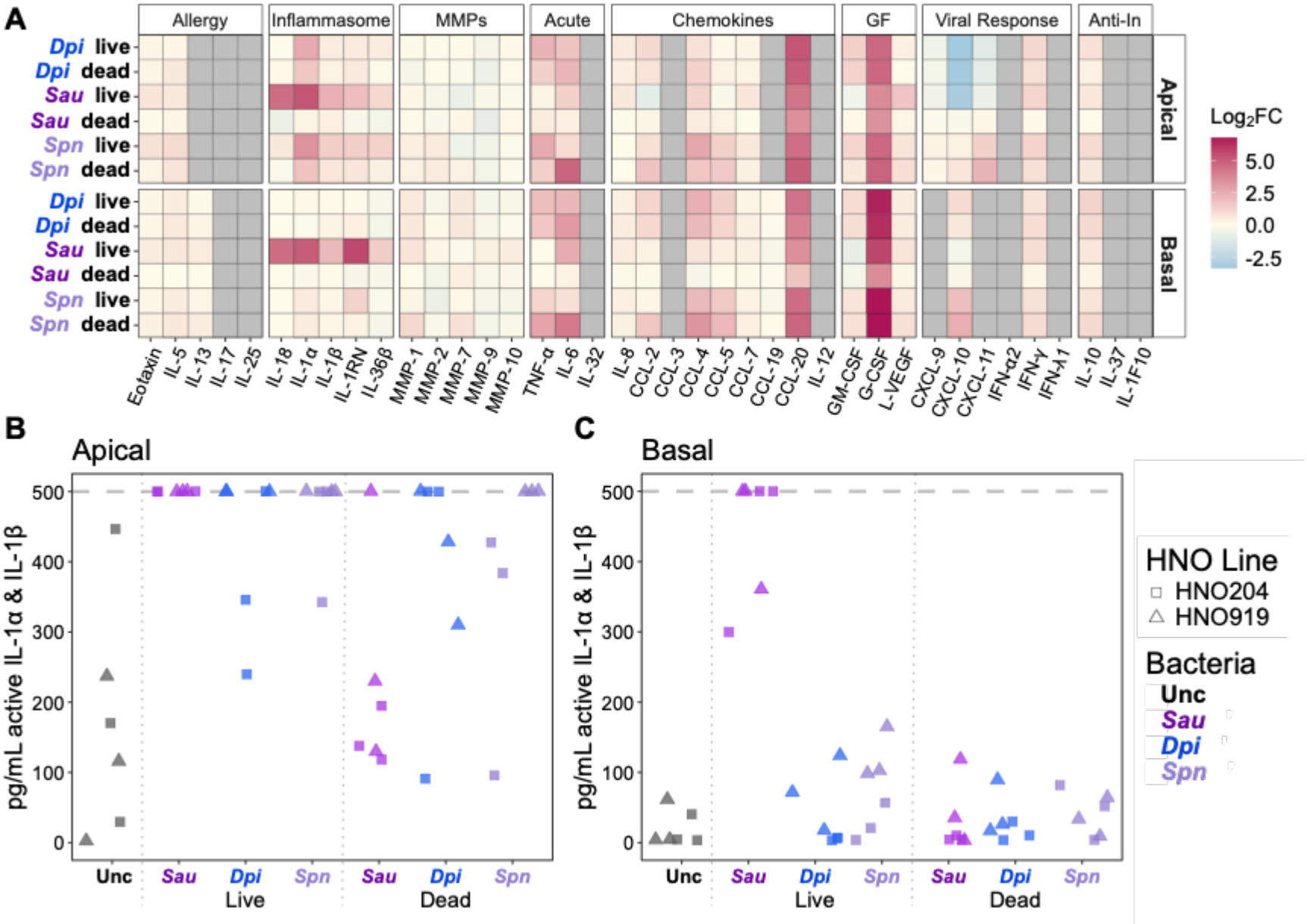
A
Allergy
Inflammasome
MMPs
Acute
Chemokines
GF
Viral Response
Anti-In
Dpi live
Dpi dead
Sau live
Sau dead
Spn live
Spn dead
Apical
Basal
Log2FC
5.0
2.5
0.0
-2.5
Eotaxin
IL-5
IL-13
IL-17
IL-25
IL-18
IL-1α
IL-1β
IL-1RN
IL-36β
MMP-1
MMP-2
MMP-7
MMP-9
MMP-10
TNF-α
IL-6
IL-32
IL-8
CCL-2
CCL-3
CCL-4
CCL-5
CCL-7
CCL-19
CCL-20
IL-12
GM-CSF
G-CSF
L-VEGF
CXCL-9
CXCL-10
CXCL-11
IFN-α2
IFN-γ
IFN-λ1
IL-10
IL-37
IL-1F10
B
Apical
pg/mL active IL-1α & IL-1β
500
400
300
200
100
0
Unc
Sau
Dpi
Spn
Sau
Dpi
Spn
Live
Dead
C
Basal
pg/mL active IL-1α & IL-1β
500
400
300
200
100
0
Unc
Sau
Dpi
Spn
Sau
Dpi
Spn
Live
Dead
HNO Line
HNO204
HNO919
Bacteria
Unc
Sau
Dpi
Spn

Figure S2. **HNOs produce general and species-specific cytokine responses to bacterial colonization, including IL-1 receptor activation in response to live S. *aureus*.** (**A**) The heatmap shows the $\log_2$-fold change of the ratio between the average amount of each cytokine detected in an apical wash or in the basal medium of HNOs monocolonized with live or dead (gamma irradiated) bacteria compared to the uncolonized control at 48 h of colonization at 34 °C. Gray tiles indicate levels below the limit of detection (**Table S1C**). IL-12 is IL-12p70. MMPs are matrix metalloproteinases. GF is growth factors. Anti-In is anti-inflammatory. (**B**) The apical and (**C**) basal IL-1α and IL-1β detected in the cytokine assays in Figure 2A is biologically active. HEK-Blue™ IL-1R Cells were used to detect catalytically active IL-1α and IL-1β produced by HNOs in the same apical washes and basal medium samples used for Figure 2. Recombinant IL-1β was used to construct a standard curve to determine pg/mL of active IL-1α and IL-1β in HNO samples. The upper limit of detection of the assay was 500 pg/mL, denoted by the gray dashed line. For A, B, and C, data are from three independent experiments in each of two HNO lines (HNO204, HNO919).

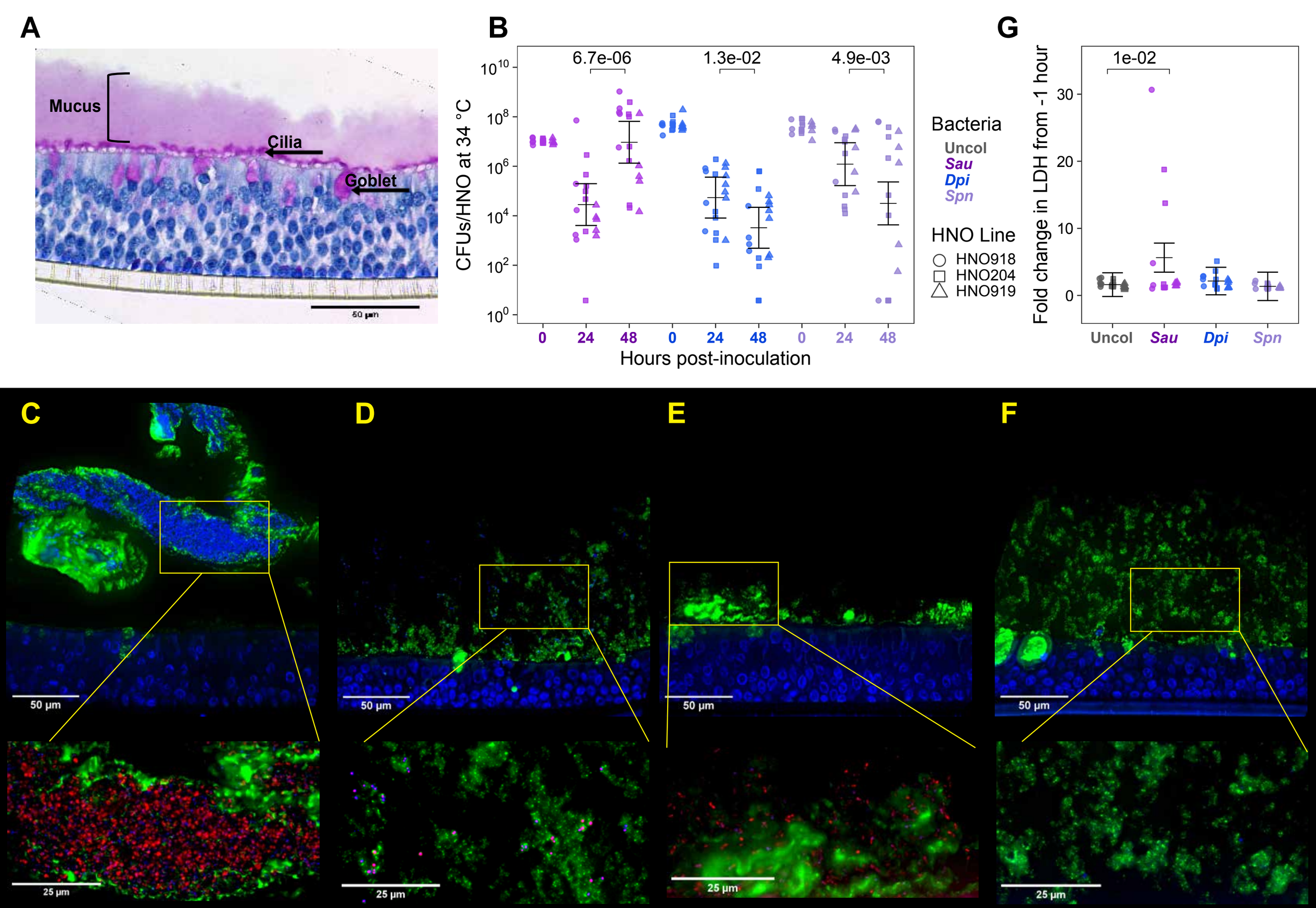
A
Mucus
Cilia
Goblet
50 µm
B
6.7e-06
1.3e-02
4.9e-03
CFUs/HNO at 34 °C
10^{10}
10^{8}
10^{6}
10^{4}
10^{2}
10^{0}
0
24
48
0
24
48
0
24
48
Hours post-inoculation
Bacteria
Uncol
Sau
Dpi
Spn
HNO Line
HNO918
HNO204
HNO919
G
1e-02
Fold change in LDH from -1 hour
30
20
10
0
Uncol
Sau
Dpi
Spn
C
D
E
F
50 µm
25 µm

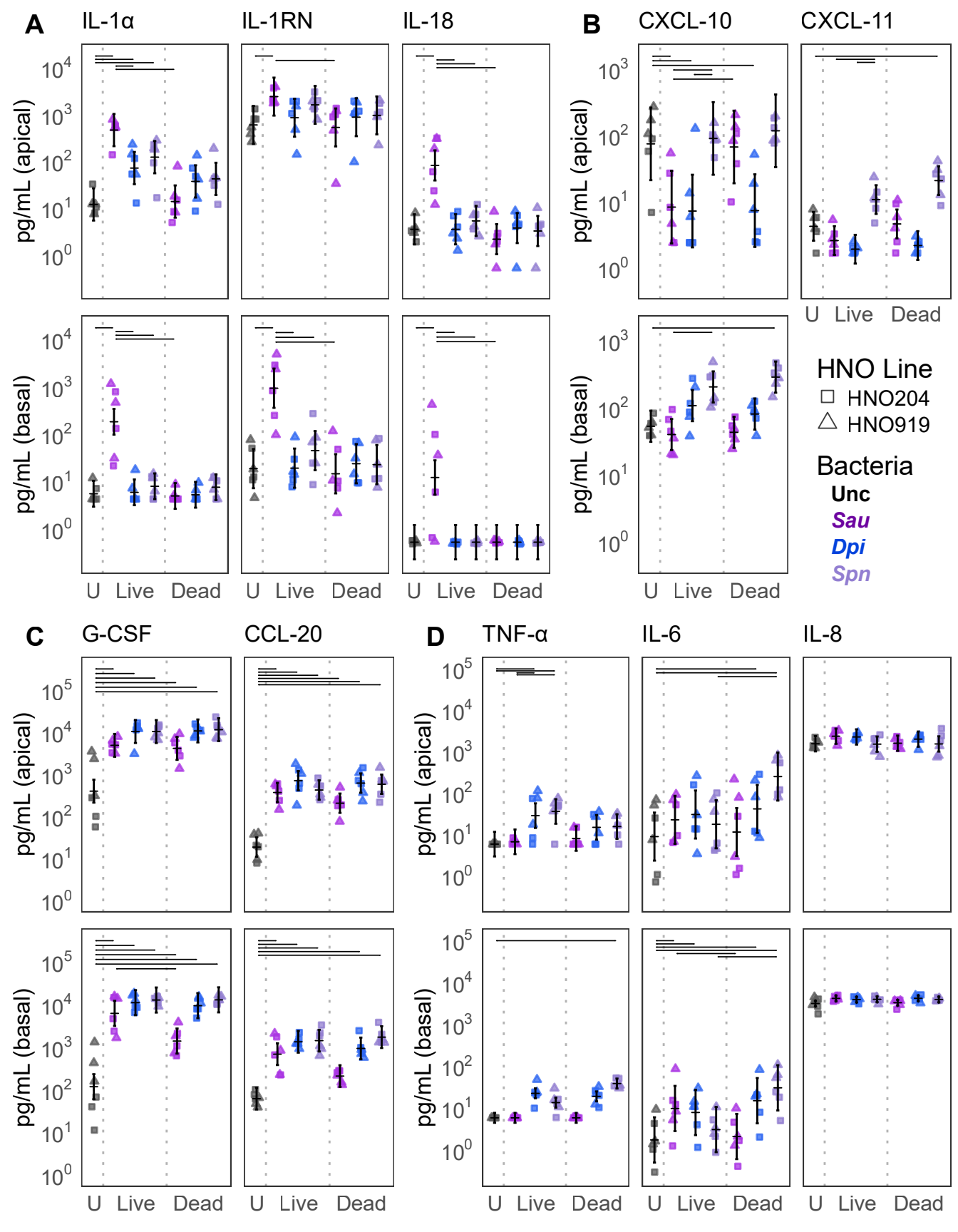
A
IL-1α
IL-1RN
IL-18
B
CXCL-10
CXCL-11
C
G-CSF
CCL-20
D
TNF-α
IL-6
IL-8
pg/mL (apical)
pg/mL (basal)
U
Live
Dead
HNO Line
HNO204
HNO919
Bacteria
Unc
Sau
Dpi
Spn

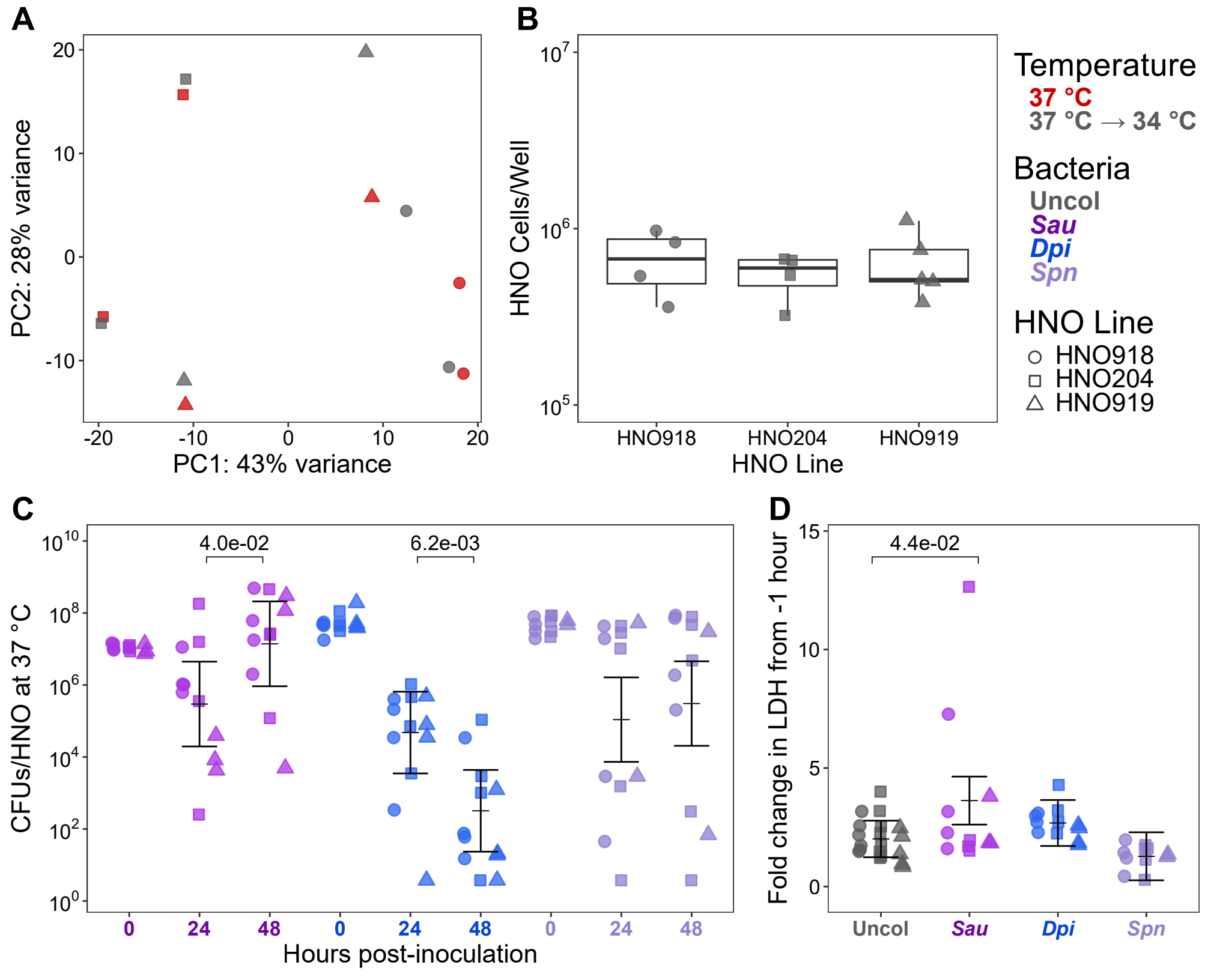
A
PC2: 28% variance
PC1: 43% variance
20
10
0
-10
-20
-10
0
10
20
B
HNO Cells/Well
10^7
10^6
10^5
HNO918
HNO204
HNO919
HNO Line
Temperature
37 °C
37 °C → 34 °C
Bacteria
Uncol
Sau
Dpi
Spn
HNO Line
HNO918
HNO204
HNO919
C
CFUs/HNO at 37 °C
10^{10}
10^8
10^6
10^4
10^2
10^0
4.0e-02
6.2e-03
0
24
48
0
24
48
0
24
48
Hours post-inoculation
D
Fold change in LDH from -1 hour
15
10
5
0
4.4e-02
Uncol
Sau
Dpi
Spn

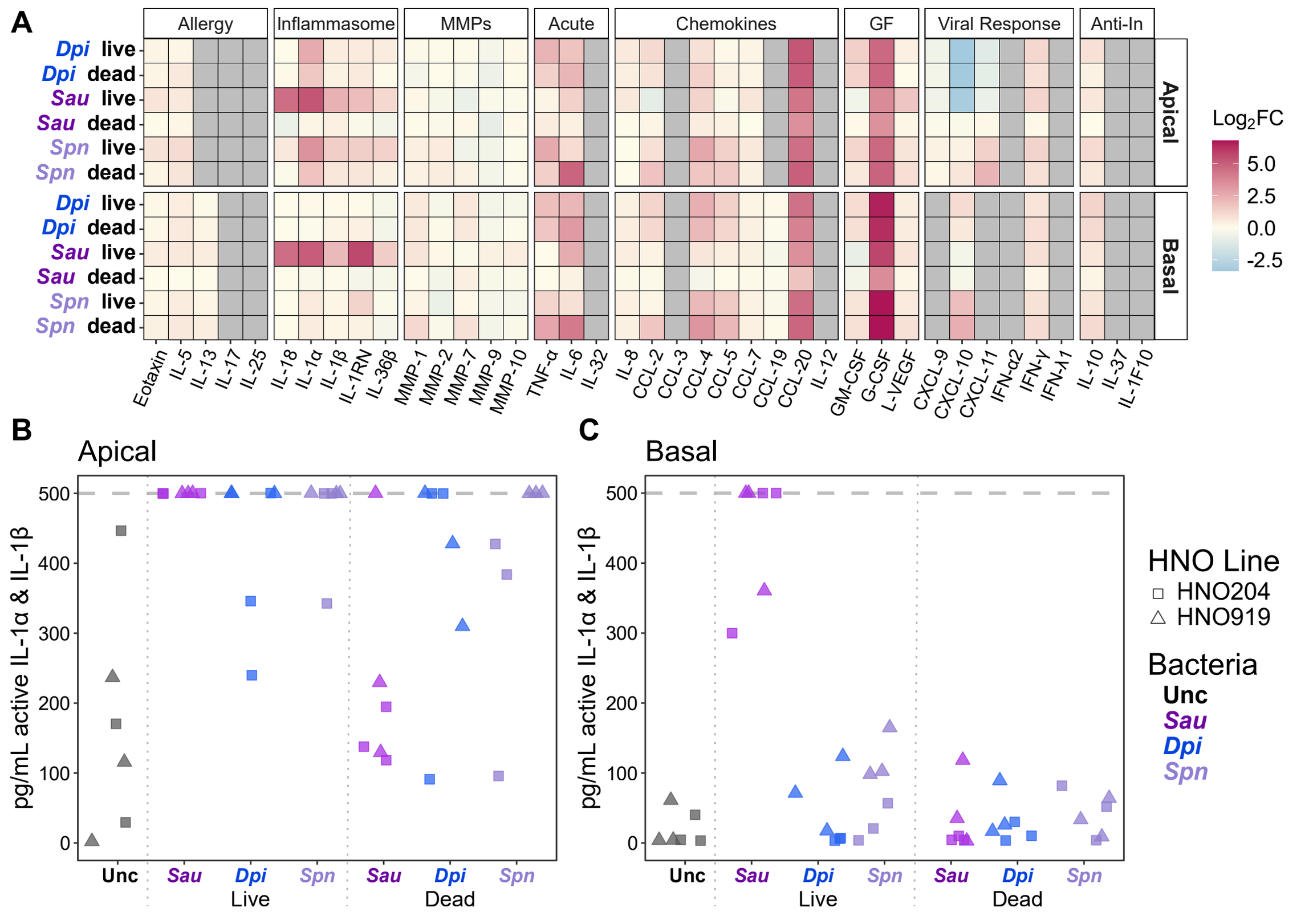
A
Allergy
Inflammasome
MMPs
Acute
Chemokines
GF
Viral Response
Anti-In
Dpi live
Dpi dead
Sau live
Sau dead
Spn live
Spn dead
Apical
Basal
Log2FC
5.0
2.5
0.0
-2.5
Eotaxin
IL-5
IL-13
IL-17
IL-25
IL-18
IL-1α
IL-1β
IL-1RN
IL-36β
MMP-1
MMP-2
MMP-7
MMP-9
MMP-10
TNF-α
IL-6
IL-32
IL-8
CCL-2
CCL-3
CCL-4
CCL-5
CCL-7
CCL-19
CCL-20
IL-12
GM-CSF
G-CSF
L-VEGF
CXCL-9
CXCL-10
CXCL-11
IFN-α2
IFN-γ
IFN-λ1
IL-10
IL-37
IL-1F10
B
Apical
C
Basal
pg/mL active IL-1α & IL-1β
500
400
300
200
100
0
Unc
Sau
Dpi
Spn
Live
Dead
HNO Line
HNO204
HNO919
Bacteria
Unc
Sau
Dpi
Spn